REVIEW

Check for updates

Hypercrosslinked polymer by an external crosslinker strategy: formation mechanism, structural regulation and applications

Zhengyang Liu,[a,b] Tao Yang,[a] Yan Song, (ID) *[a,b] Ning Zhao, (ID) [c] Shijie Wu,[a] Zihui Ma,[a,b] Xiangjie Gong,[a,b] Xiaodong Tian (ID) [a,b] and Zhanjun Liu (ID) [a,b]

Hypercrosslinked polymers (HCPs) are a type of porous organic polymer that have been rapidly developed over the past few decades. These polymers are primarily synthesized through Friedel–Crafts alkylation over Lewis acid catalysts such as ferric chloride and aluminum chloride, leading to the formation of porous materials by cross-linking. HCPs can be prepared through strategies such as post-cross-linking of polystyrene-type polymer precursors, self-cross-linking of specific aromatic monomers, and cross-linking by external agents with aromatic monomers. Among these methods, the external cross-linking approach has been utilized in fields such as gas storage, adsorption, catalysis, separation, and energy storage due to its mild synthesis conditions, good stability, high yield, broad availability of monomers, and tunable structure. In this paper, recent research progress in the preparation of HCPs by external cross-linking methods, with a focus on the formation mechanisms, structural regulation, and applications, is reviewed. Additionally, the drawbacks and challenges while projecting future developments in HCPs are highlighted.

[a]Shanxi Key Laboratory of Carbon Materials, Institute of Coal Chemistry, Chinese Academy of Sciences, Taiyuan 030001, China. E-mail: yansong1026@126.com
[b]Center of Materials Science and Optoelectronics Engineering, University of Chinese Academy of Sciences, Beijing 100049, China
[c]State Key Laboratory of Coal Conversion, Institute of Coal Chemistry, Chinese Academy of Sciences, Taiyuan 030001, China

1 Introduction

Porous organic polymers (POPs), a branch of porous materials, have been intensively developed in recent decades due to the characteristics of a high specific surface area, tunable pore structure and excellent chemical stability.[1] POPs mainly include covalent organic frameworks (COFs),[2–4] conjugated microporous polymers (CMPs),[5,6] polymers of intrinsic microporosity (PIMs),[7,8] and hypercrosslinked polymers (HCPs).[9,10] However, the synthesis of CMPs, COFs and some other organic

Zhengyang Liu is currently pursuing his Ph.D. degree at the University of Chinese Academy of Sciences under the supervision of Prof. Yan Song. His research interests focus on polymer-derived carbon and functional carbon materials.

Zhengyang Liu

Yan Song is a professor at the Institute of Coal Chemistry, Chinese Academy of Sciences. She is engaged in the preparation and application of carbon materials.

Yan Song

porous materials requires the use of noble metal catalysts, complex monomer units, or severe reaction conditions.[11] Therefore, the low-cost controllable synthesis of organic porous materials remains a challenge.

Hypercrosslinked polymers (HCPs) are a class of polymer consisting of light elements such as C, H, O, and N, connected by stable covalent bonds which are highly crosslinked porous organic polymers based on the Friedel–Crafts alkylation catalyzed by Lewis acid (*e.g.*, FeCl_3 or AlCl_3). The synthesis of HCPs utilizes the concept of "cross-linking" commonly used in materials science, where the polymer network is designed with a rigid structure to prevent the polymer chains from contracting tightly, thereby forming permanent pores between the molecular chains.[12,13] The polymers generally possess a stable pore structure and high degree of designability, allowing precise control of the specific surface area (SSA), pore structure, functional groups, and even the morphology. Over decades of development, various monomers with diverse structural properties have been used, resulting in an increasing variety of HCPs that have been widely utilized in the fields such as gas adsorption and storage, catalysis, and energy storage.[12,14–17]

Currently, there are three primary methods for the synthesis of HCPs: the post-crosslinking, self-crosslinking, and external crosslinking methods. Different synthesis strategies result in HCPs with varying structures.

The post-crosslinking method, first reported by Davankov in 1980,[18] usually led to a stable pore structure and high SSA (600–2000 m^2 g^{-1}).[19] The pore size decreased as the degree of cross-linking increased. Many studies had focused on post-crosslinking method for HCPs.[20–24] High specific surface area divinylbenzene-based HCPs and CMP-based hyper-crosslinked polymers (KCMPs) could be prepared by multi-step crosslinking.[25,26] Furthermore, specific elements could be introduced to the polymer skeleton or micro/nano-particles to improve the functionalization of the polymer.[27,28] The functional groups, such as alkyl groups,[29] amine groups,[30,31] nitro groups,[32,33] phenolic hydroxyl groups,[34] and carboxyl groups,[35] could increase the polarity of the polymer, thereby enhancing the adsorption properties of the polymer. Although hypercrosslinked resins possess a high SSA and good stability, the synthesis processes are complicated, involving a long time and high precursor requirements. Precise design of the precursor is often necessary to obtain the crosslinked network structure. The structure and performance of the product are significantly affected by the precursor. Therefore, the method has certain limitations for practical applications which restricts the rapid development.

Synthesis of HCPs through different strategies has been the focus of recent efforts. Consequently, researchers have gradually developed a method for preparing HCPs using precursor-self-crosslinking methods. This innovation provided a new approach for creating rigid porous polymers, with greater diversity in polymer networks. Extensive research has been conducted on the synthesis of hypercrosslinked polymers (HCPs), utilizing halogenated compound monomers such as

p-xylene,[36,37] α,α′-dichloro-*p*-xylene (DCX), 4,4′-bis(chloromethyl)-1,1′-biphenyl (BCMBP),[38] and 9,10-bis(chloromethyl) anthracene (BCMA).[39] However, this method presents certain limitations in terms of monomer selection or the requirement for specific catalysts and solvents. These requirements, while enabling precise control over the polymer architecture and functionality, inevitably escalate the cost of producing HCPs. Additionally, monomers containing chloromethyl functional groups will generate hydrogen chloride gas during the reaction, causing damage to the environment and equipment. Therefore, methods that do not require specific functional monomers or can utilize polymers with multiple reactive groups are necessary.

The external crosslinking method involves suitable crosslinking agents that interlink aromatic monomers, to obtain a porous polymer skeleton. Generally, aromatic compounds such as benzene, biphenyl, triphenylbenzene, naphthalene, anthracene, and phenanthrene are used as monomers. This method, pioneered by Tan's group in 2011, represents a new strategy and leads to major breakthroughs in the development of HCPs. In this method, aromatic monomers such as benzene and biphenyl can be "woven" into a rigid network in a single step by adding an external crosslinking agent, such as formaldehyde dimethyl acetal (FDA), catalyzed by a Lewis acid. The process enables the generation of polymers with pore structures, functional groups, and desirable properties by connecting different building blocks.[14,40] Cooper *et al.* concluded that the external crosslinking method broadens the choice of monomers, significantly reduces the production costs and offers advantages in material design.[41,42]

Due to the advantages of flexibility, diversity, a wide source of monomers, and suitability for large-scale production, the external crosslinking method has flourished in recent years. Compared with the post-crosslinking and self-crosslinking methods, the monomers used in this method do not require specific functional groups. Additionally, the SSA and pore size of HCPs can be adjusted by modifying the proportion of the feed material, the type of crosslinking agent, and the monomers. Moreover, the functionalization of HCPs can be realized by using monomers containing functional groups, which promotes the range of practical applications.

This paper primarily reviews the recent research progress on the preparation of HCPs based on the Friedel–Crafts alkylation by the external crosslinking method, which focuses on the formation mechanism, the structural modulation (pore structure and heteroatomic groups) as well as the application in gas adsorption, purification, separation, catalysis and energy storage. Additionally, the drawbacks in the development of HCPs and future prospects are proposed.

2 Mechanism of formation of HCPs

Some research on the formation mechanism of HCPs was reported. The polymerization of HCPs is fundamentally based on the Lewis acid-catalyzed Friedel–Crafts alkylation reaction

© 2025 The Author(s). Published by the Royal Society of Chemistry

RSC Appl. Polym., 2025, **3**, 746–766 | **747**

via a one-step process. However, the Friedel–Crafts reaction occurs multiply and randomly throughout the process. Due to the complexity of the process, the study of the formation mechanism is challenging.

Tan *et al.* regulated the structure of HCPs by adjusting the content of DVB in the diethylenebenzene–vinylbenzyl chloride (DVB–VBC) precursor.[43] The results showed that as the DVB content gradually increased within the range of 0–10%, the pore size of the HCPs decreased. The pore size distribution gradually narrowed. Thereby, they proposed a possible reaction mechanism: for polymer precursors without DVB, solvents completely dissolved the molecular chains, to form a disordered configuration. The chloromethyl functional groups on the phenyl rings were more likely to interact with the phenyl rings in distant molecular chains. During the crosslinking reaction, distantly positioned phenyl rings connected to form larger voids, eventually developing into large pore structures. When the DVB content was high, DVB stabilized the initial crosslinking process. The molecular chains were maintained in an extended state, with the phenyl rings crosslinking only with adjacent phenyl rings. As a result, the crosslinking structure was more uniform and the pore structure was more homogeneous. This provided guidance for the regulation of the pore structure of HCPs. The exploration of polymer structures remained a focus in materials science. By utilizing the non-oxidizing catalyst $SnCl_4$ to copolymerize styrene-0.5% DVB and chloromethyl ether, Davankov *et al.* further investigated the structure and crosslinking degree of the polymers.[44] In the hyper-crosslinked polystyrenes, the structure lacked carbonyl functional groups. Each phenyl ring in the polymer structure connected to the adjacent phenyl ring through 3, 4, or 5 methylene units, forming an extremely rigid and highly interconnected network.

Kim *et al.* synthesized HCPbPh *via* Friedel–Crafts polyalkylation catalyzed by $FeCl_3$, using biphenyl as monomer and FDA as crosslinker. The possible polymerization mechanism was proposed (Fig. 1a).[45] In DCE solvent, the $FeCl_3$ first formed an electron-deficient center on the FDA carbon atoms. The generated carbocationic species was subsequently attacked by the benzene rings in bPh, producing methanol as byproduct. These highly active intermediates were then converted into methylene bridge bonds through reactions with other bPh molecules, leading to the formation of a rigid hypercrosslinked polymer network. Xu *et al.* proposed that HCPs could be rapidly synthesized through electron donation induction, where donor groups on the monomer generated numerous electrophilic sites, thereby significantly enhancing the crosslinking of BCMBP monomers.[48] High-SSA HCPs could be prepared with the assistance of ball milling. The mechanism for rapid polymerization includes donor groups generating additional active sites for fast self-crosslinking, and solvent enhancing the SSA of the crosslinked network while ball milling facilitates uniform reactions to accelerate the overall reaction rate. Liu *et al.* constructed HCPs from waste PS and further elucidated the mechanism of the crosslinking reaction (Fig. 1b).[46] The benzene rings in the PS skeleton formed an intermediate through reaction with FDA under the Lewis acid catalyst $FeCl_3$, producing methanol as a byproduct. The inter-
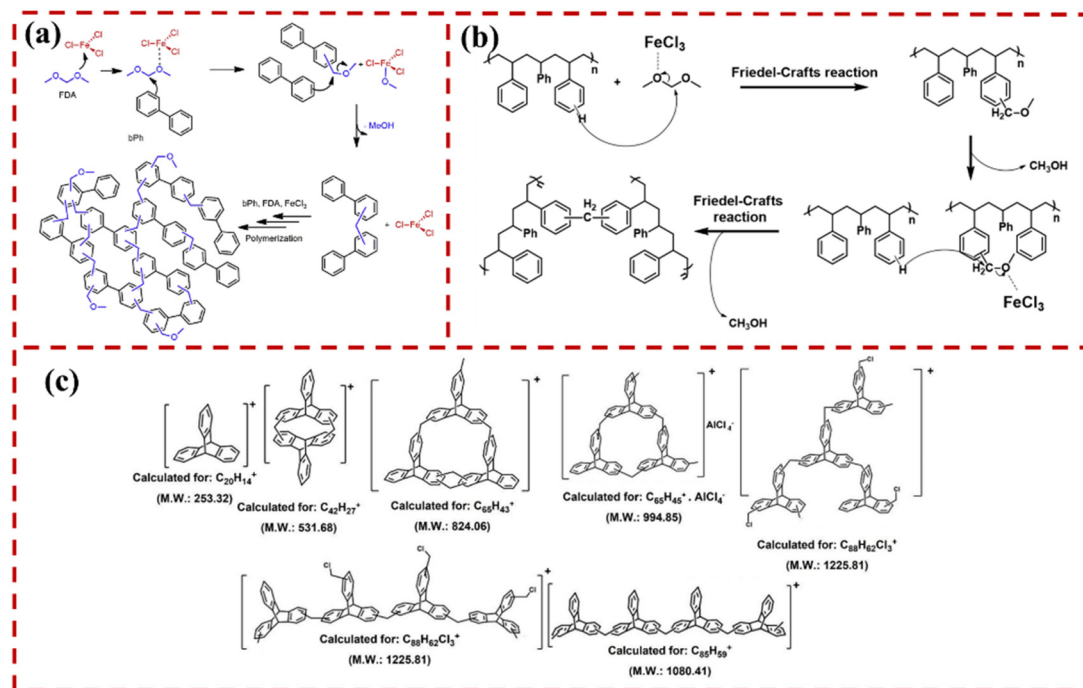

Fig. 1 (a) Synthesis pathway: polymerization of HCP *via* FDA as crosslinker.[45] Copyright 2021, Elsevier. (b) Proposed mechanism of polystyrene-based hypercrosslinked polymer.[46] Copyright 2020, Elsevier. (c) Solvent knitting polymerization: MALDI–TOF analysis of the samples obtained after 30 min.[47] Copyright 2022, American Chemical Society.

© 2025 The Author(s). Published by the Royal Society of Chemistry

mediate then underwent substitution with hydrogen atoms on another PS unit, completing the crosslinking reaction. Due to the robustness and fast kinetics of the Friedel–Crafts alkylation reaction, the hypercrosslinking reaction yielded a high-SSA porous nanostructure with excellent stability.

Moreover, the reasons for the formation of nanopores have not been definitively elucidated and are infrequently reported in the literature. In 2022, Patra's group synthesized an HCP (SKTP) using tris-benzene building units *via* a solvent-knitting reaction. The HCP exhibited a wheel-like topology and an "internal free volume" of 31 $Å^3$.[47] The molecular structure of the oligomers was determined using MALDI-TOF analysis of the reaction mixture after 30 minutes (Fig. 1c). The optimized oligomeric model structure was employed. The results suggested that the cross-linking reaction occurred at the β position of the tris-benzene. Further simulation studies indicated that pores of 0.6 and 0.9 nm were formed. The cross-linking bridge bonds between polymer chains resulted in voids ranging from 1.4 to 2 nm. The simulated structure aligned with the pore size analysis obtained from N_2 adsorption/desorption, corroborating the rationale for the formation of the pore structure in HCPs.

3 Structural modulations of HCPs

In recent years, researchers have conducted extensive studies on the synthesis of HCPs using the external crosslinking method, by utilizing crosslinking agents of formaldehyde dimethyl acetal (FDA), *p*-methoxybenzene, and other compounds.[16,49–51] Moreover, HCPs could be prepared by using monomers with aryl ring structures and their derivatives, with formaldehyde dimethyl acetal (FDA) as crosslinking agent. The molecules of constructed monomers using FDA as crosslinker were shown in Fig. 2. The approach significantly expanded the range of monomers available for the preparation of HCPs, advancing the development of HCP synthesis.

Currently, the structural modulation of HCPs primarily involves two aspects: the modulation of the SSA and the incorporation of functional groups (or specific elements). Various methods were adopted. One was modulating the microstructure of HCPs by changing the reagents (monomers, crosslinkers, and solvents) and the ratio of reactants in the synthesis system. Another approach was to introduce heteroatomic groups, which employed modification strategies to prepare HCPs with distinct functions.
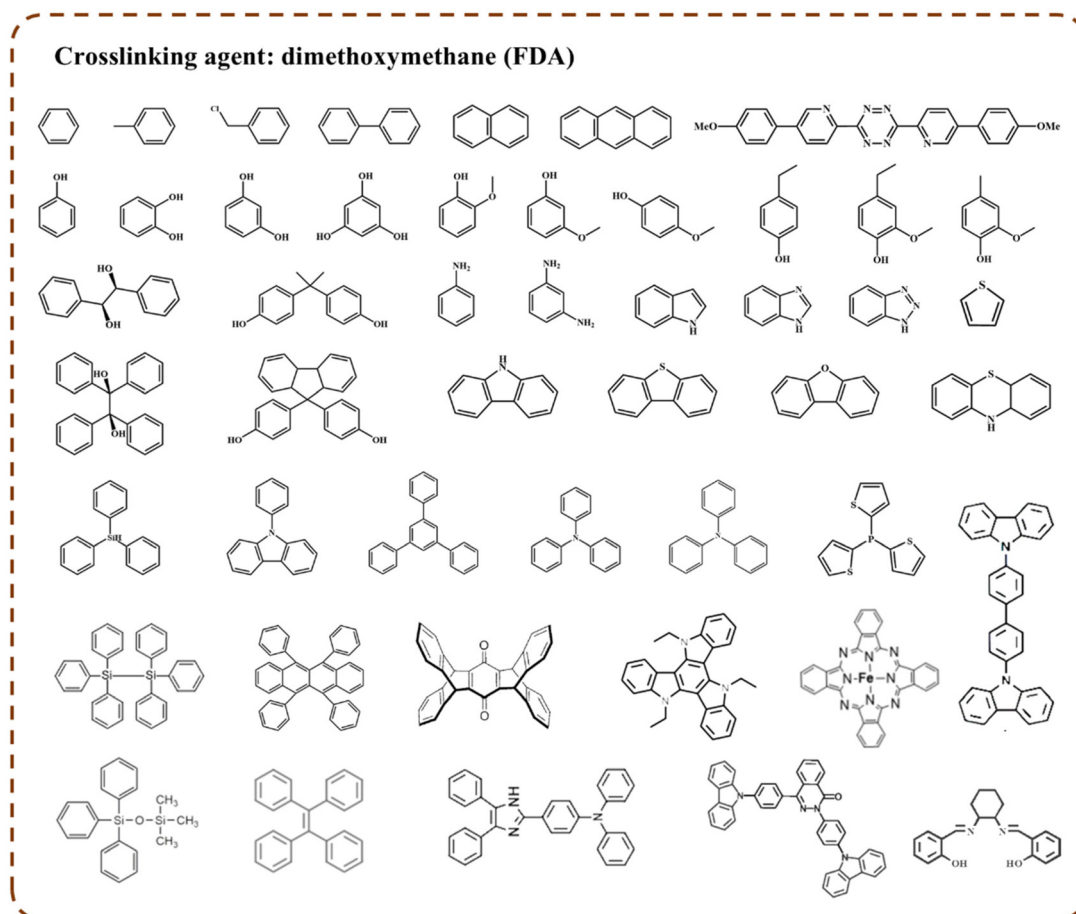

Fig. 2 Monomers for external crosslinking reaction (1,2-dichloroethane as solvent, FDA as crosslinking agent, FeCl₃ as catalyst).

© 2025 The Author(s). Published by the Royal Society of Chemistry

RSC Appl. Polym., 2025, **3**, 746–766 | **749**

In the case of the simplest compound, benzene, the specific surface area of HCPs can be directly modulated by grafting functional groups through monomers. For example, when FDA is used as the cross-linking agent and 1,2-dichloroethane (DCE) as the solvent, the SSA of HCPs with aniline as monomer was only 7 m^2 g^{-1}.[42] However, when the functional group is trimethyl silane, the SSA was 1299 m^2 g^{-1}, which is essentially comparable to that of the benzene monomer HCPs (1289 m^2 g^{-1}).[52] Furthermore, when the ratio of benzene to aniline was regulated for the cross-linking reaction, the specific surface area of HCPs gradually decreased with the increase of aniline addition. This suggests that by changing the above conditions, the structure of HCPs can be further designed for the purpose of optimizing the structure of HCPs.

3.1 Specific surface area and pore structure modulation

The most commonly reported cross-linking agent was FDA. The data on the SSA, pore structure, and application of HCPs prepared using FDA as cross-linking agent, FeCl$_3$ as catalyst, and 1,2-dichloroethane (DCE) as solvent were summarized in Table 1. It was evident that HCPs with SSA ranging from 3 m^2 g^{-1} to approximately 1400 m^2 g^{-1} could be simply constructed by selecting different monomers.

3.1.1 Monomers. HCPs with diverse structures can be effectively constructed by utilizing different monomers. For example, Li et al. synthesized HCPs with abundant porosity and high thermal stability using α,α′-dichloro-p-xylene (DCX) and α,α′-dibromo-p-xylene (DBX) via a cross-linking reaction (Fig. 3). The SSA was 1418 and 1219 m^2 g^{-1} with corresponding total pore volumes of 1.815 and 1.789 cm^3 g^{-1}, respectively.[99] Due to the abundant porosity, HCPs were modified by polyvinyl alcohol (PVA) and coated with polypyrrole (PPy) and silver nanoparticles as a sunlight-absorbing layer. The resulting material, Ag/PPy-PVA-HCPs, demonstrates excellent surface wettability, low thermal conductivity, and high optical absorption.

HCPs were constructed from a variety of monomers. In external crosslinking reactions, monomers ranging from the simple aromatic ring monomer, benzene, to phenyl derivatives, polycyclic aromatic hydrocarbons, and complex heterocyclic compounds can be used. Monomers or substituent groups of the monomers might affect the structure of HCPs. Ghaemi et al. prepared HCPs with mesoporous structures using benzene as monomer, achieving an SSA of 572 m^2 g^{-1}, which served as an effective adsorbent for CO$_2$.[79] Li et al.[77] modulated the morphology of HCPs based on Jiang's work[100] by using toluene as monomer and formaldehyde dimethyl acetal (FDA) as cross-linker. HCPs with benzene as monomer exhibited morphologies of nanoparticles and nanotubes with an SSA of 773 m^2 g^{-1} and pore volume of 0.96 cm^3 g^{-1}. In contrast, HCPs with toluene as monomer were nanotubes whose SSA and pore volume were 719 m^2 g^{-1} and 0.58 cm^3 g^{-1}, respectively. Yao et al. used a series of phenyl compounds as monomers (benzene, chlorobenzene, toluene, phenol, etc.) to prepare HCPs via FDA crosslinking.[101] The results showed that the absence of substituent groups on the benzene monomers reduced the steric hindrance, leading to higher reactivity.

This increased the degree of cross-linking and consequently the SSA of the HCPs. It was evident that monomers with different substituent groups affected the SSA and microstructures of HCPs. Wang et al. modulated the SSA of HCPs by FDA crosslinking using substituted and unsubstituted phenylboronic acids (PBAs) as monomers.[81] The product derived from unsubstituted PBAs achieved an SSA higher than 909 m^2 g^{-1}. However, the SSA of HCPs prepared by substituted PBAs with different groups as monomers drastically decreased (<80 m^2 g^{-1}), thereby reducing the adsorption properties of the material. Therefore, it was crucial to maintain both the functionalized and porous structures of HCPs simultaneously.

By copolymerization of benzene with heterocyclic compounds using FDA crosslinking, it was possible to tune the functional and structural properties of the HCPs. Liu et al. prepared HCPs-bipy samples using benzene and 2,2′-bipyridine as monomers through Friedel–Crafts alkylation and Scholl coupling reactions.[67] The as-synthesized HCPs exhibited an SSA of 1027 m^2 g^{-1}, about twice that of the Friedel–Crafts alkylation product. Additionally, porous HCPs could be prepared using substituted polycyclic aromatic naphthalene as monomer. Kim et al. prepared porous polymers using 2-naphthol (p2NPh-OH) as monomer and obtained solid acid catalysts through further functionalization with sulfonic acid.[102] The SSA of p2NPh-OH reached 408 m^2 g^{-1}. While that of p2NPhO-SO$_3$H was reduced to 180 m^2 g^{-1}, indicating that the functional groups in HCPs could reduce the SSA.

Cabello et al. prepared HCPs by FeCl$_3$-catalyzed crosslinking of biphenyl monomers with FDA, with the catalyst retained in the final material.[103] They further prepared magnetic hybrid hypercrosslinked polymer-derived carbon@MOF (C-BHCP@MIL-100(Fe)) through a hydrothermal reaction. By controlling the conversion ratio of the iron particles to MIL-100(Fe) through the reaction time, the SSA of C-BHCP@MIL-100(Fe) was controlled between 314–687 m^2 g^{-1} and the pore volume was between 0.43–0.488 cm^3 g^{-1}. Longer reaction times resulted in a higher SSA and pore volume. Increasing the conjugation degree of phenyl monomers significantly enhanced the efficiency of HCPs in photogenerated carrier separation and conversion. HCPs with different conjugation degrees could be prepared by Friedel–Crafts alkylation using benzene (BE), diphenyl (DP), p-terphenyl (TP), or p-quaterphenyl (QP) as monomers. The SSA of HCPs tended to decrease as the degree of conjugation increased. HCPs constructed with DP as the monomer had the highest SSA (743.1 m^2 g^{-1}), much larger than HCPs with QP as the monomer (558.9 m^2 g^{-1}). HCPs with BE as monomer showed the highest microporous content (45.1%). Thus, the structure of HCPs could be effectively modulated using monomers with different conjugation degrees.[74]

Horike et al. synthesized HCPs with various structures via a low-cost, solvent-free ball milling approach, thereby avoiding the use of conventional toxic solvents.[104] Additionally, they prepared HCPs by modified ball milling based on the Scholl coupling reaction using FDA-free reagents. Under optimized conditions, HCPs with SSAs of 626 m^2 g^{-1} and 782 m^2 g^{-1} were obtained with benzene and triphenylbenzene as mono-

750 | RSC Appl. Polym., 2025, 3, 746–766

© 2025 The Author(s). Published by the Royal Society of Chemistry

Table 1 Summary of the preparation of HCPs by an external crosslinking method

No.	HCPs	Monomers	S_{BET} (m^2 g^{-1})	$V_{micro} : V_{total}$	Applications	Ref.
1	HCP	Catechol	3	—	Water treatment	53
2	MPD-HCP	m-Phenylenediamine	77 (AlCl$_3$)	—	Water treatment	54
3	NH$_2$-HCPs	m-Phenylenediamine	77	—	CO$_2$/N$_2$ separation	55
4	HCP-P	Phenol	183	— : 0.227	Cs$^+$ adsorption	56
5	HCPs	Phenothiazine	209	—	Iodine capture	57
6	SSHCP-1	Cassava starch and styrene	222	0.08 : 0.21	Water treatment	58
7	TBHCP-OH	2,6,14-Triaminotriptycene and phenol	235	— : 0.066	CO$_2$ capture	59
8	HCP-4	4-Ethylphenol	247	0.02 : 0.23	CO$_2$ capture	60
9	PPT	Tris(2-thienyl)phosphine and thiophene	282	—	Nitroarene reduction	61
10	N-HCPTs	Triphenylamine	370	—	Energy storage	62
11	FePc-POP	Firon(II) phthalocyanine and biphenyl	427	—	Heterogeneous catalyst	63
12	SA-MMNPs	Fe$_3$O$_4$@poly(styrene-co-sodium acrylate)	485	0.09 : 0.64	Water treatment	64
13	PHCP	Pitch	531	0.151 : 0.455	Ag$^+$ adsorption	65
14	HPOP-3	$Meso$-Hydrobenzoin (MHB) and 1,1,2,2-tetraphenyl-1,2-ethanediol (TPED)	552	— : 0.496	Water treatment	66
15	HCPs-bipy	Benzene and 2,2′-bipyridine	564	0.12 : —	Catalytic	67
16	HCP	Benzene	572	0.096 : 0.871	CO$_2$ capture	68
17	An-CPOP-1	9,10-Bis(diphenylmethylene)-9,10-dihydroanthracene	580	— : 0.44	CO$_2$ uptake and supercapacitor	69
18	HCP	Fluorene-9-bisphenol	640	— : 0.39	Uranium(VI) adsorption	70
19	HCLRs	Chloromethylated polystyrene	650	0.18 : 0.75	Water treatment	71
20	HCPs	Fluorene-9-bisphenol	663	— : 0.41	Water treatment	72
21	PCMOP-H1	Carbazole and phthalazinone	675	0.15 : 0.49	CO$_2$, N$_2$, CH$_4$ adsorption and selectivity	73
22	HCPs	Diphenyl	743	—	Photocatalytic	74
23	Th-2	Thiophene	750	0.3 : 0.5	Water treatment	75
24	TSP-HCP-900	Carbazole	756	0.6 : —	Porous carbon for oxygen reduction reaction	76
25	P3	9-Phenylcarbazole	769	0.14 : 0.63	CO$_2$ uptake	40
26	HCP-1	Benzene	773	— : 0.96	Desalination and water purification	77
27	HCPs	4,4′-Bis(N-carbazolyl)-1,1′-biphenyl	784	0.34 : 0.45	Gas separation and storage	78
28	Poly-salen-c	Salen-c and benzene	798	0.24 : 0.48	Catalytic	61
29	HCP	Benzene	824	0.14 : —	CO$_2$ capture	79
30	HCPs	Polystyrene	853	0.14 : —	Water treatment	80
31	PBA-HCP	Phenylboronic acid (PBA)	909	— : 1.30	Chlorophenol adsorption	81
32	HCPAs	1-(Benzyloxy)-4-ethylbenzene	948	0.16 : 0.55	Water treatment	82
33	HCP-5	Benzyl alcohol (BA), 2-phenylimidazole (PID)	992	0.12 : 1.06	CO$_2$ capture	83
34	TATHCP	Triazatruxene	997	0.44 : 0.63	CO$_2$, CH$_4$, H$_2$ capture and catalytic	84
35	PHCP	Pentiptycene	1074	—	Water treatment	85
36	HCP-DH	Hexaphenyldisiloxane	1084	—	Water treatment	86
37	HCP-BZD	Benzimidazole	1088	0.27 : 1.41	Water treatment	87
38	Ph-BNPPA-HCP	1,1′-Bi-2-naphthol-derived phosphoric acid	1098	0.45 : 1.26	Asymmetric organocatalysts	88
39	HCPbPh	Biphenyl	1100	0.41 : 1.14	Pollutant adsorption and energy storage	45
40	Si-HCP-4d	Triphenylsilane	1101	0.25 : 1.24	Hydrogen storage and water treatment	89
41	HCP-S5	D/L-Phenylalanine and benzene	1101	0.31 : 1.55	D/L-Tryptophan adsorption	90
42	TZ-HCP	Benzene and 3,6-di(pyridin-2-yl)-1,2,4,5-tetrazine	1139	0.2 : 0.91	Photocatalytic	91
43	HCP	Benzimidazole and benzene	1140	0.23 : 1.28	Water treatment	92
44	A1Fe1M20	Anthracene	1173	0.36 : 0.55	H$_2$ adsorption	93
45	HCP-5	Styrofoam	1199	—	Water treatment and CO$_2$ capture	94
46	HCPs	Benzyl chloride	1249	0.197 : 1.017	CO$_2$ adsorption	95
47	HCP-TTDs	1,1,1-Trimethyl-3,3,3-triphenyldisiloxane	1285	—	Water treatment	96
48	HCP-TPB	1,3,5-Triphenylbenzene and L-tyrosine	1309	—	Determination of compounds	97
49	HCP-Rub	Rubrene	1403	—	Environmental detection	98

mers, respectively. The ssNMR results indicated that the mechanochemical method resulted in a higher degree of polymerization, leading to the formation of a porous structure. This provided an environmentally friendly approach for developing porous materials.

HCPs with a high SSA are advantageous in application. For example, 1,1,1-trimethyl-3,3,3-triphenyldisiloxane (TTD) was used to construct micro–mesoporous-structured HCPs with an SSA close to 1300 m^2 g^{-1}, which exhibited good adsorption capacity for Malachite green (2346 mg g^{-1}), Congo red (2052 mg g^{-1}), and rhodamine B (1938 mg g^{-1}).[96] Zheng et $al.$ prepared HCPs with an SSA greater than 1400 m^2 g^{-1} using rubrene as monomer.[98] The HCPs possessed an abundantly microporous structure, strong hydrophobicity, and a large conjugated structure, making them ideal candidates for efficient enrichment of polycyclic aromatic hydrocarbons (PAHs).
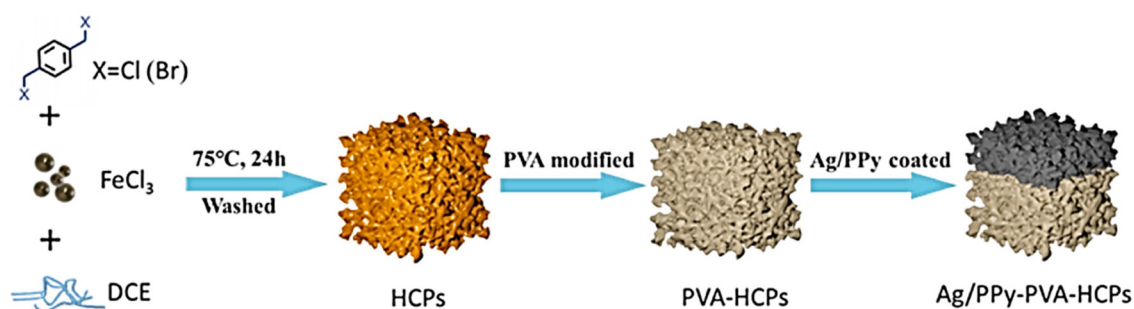
© 2025 The Author(s). Published by the Royal Society of Chemistry

RSC Appl. Polym., 2025, **3**, 746–766 | **751**

Fig. 3 Synthesis of DCX–based hypercrosslinked polymer and its functionalization.[99] Copyright 2021, Elsevier.

3.1.2 Crosslinking agents. The structure of HCPs could be modulated by varying crosslinking agents. In addition to formaldehyde dimethyl acetal (FDA), 4,4′-bis(chloromethyl)-1,1′-biphenyl (BCMBP), α,α′-dichloro-p-xylene (DCX), and 1,4-dimethoxybenzene (DMB) were also employed (Table 2). Among them, BCMBP typically resulted in HCPs with an ultra-high SSA (close to 2000 m^2 g^{-1}). It was also used to link monomers, for the preparation of HCPs with enhanced-SSA-containing functional group-substituted monomers. The HCP (SSHCP-3), synthesized with starch-graft-styrene copolymer as monomer and crosslinked by BCMBP, achieved the highest SSA of 818 m^2 g^{-1}, with an essentially equivalent micro–mesoporous structure.[58] Additionally, BCMBP was used to link benzene monomers with hydroxyl groups (–OH) at different substituent positions (phenol, hydroquinone, and phloroglucinol), resulting in hydroxyl-functionalized HCPs (HCP-POL, HCP-HQ, and HCP-PG) with an SSA of 756, 1055, and 773 m^2 g^{-1}, respectively.[105] The HCP-HQ had the average median pore width of 2.27 nm and the total pore volume of 0.51 cm^3 g^{-1}.

Huang *et al.* synthesized HCPs using α,α′-dichloro-p-xylene (DCX) and α,α′-dibromo-p-xylene (DBX) as cross-linking agents, with benzimidazole as monomer.[110] The SSA of the synthesized HCPs varied significantly depending on the substi-

tution ions of the cross-linking agents. The SSA of the HCPs prepared using DCX (HCP-Cl) reached 1063 m^2 g^{-1}, while that of DBX (HCP-Br) was significantly lower (exact value missing). Additionally, the microporous volume of HCP-Cl was substantially higher than that of HCP-Br. The difference was attributed to the higher stability of $FeCl_4^-$ compared with $FeCl_3Br^-$ which enhanced the cross-linking of DCX, offering new insights into the regulation of the SSA and pore structure of HCPs. Furthermore, they established a general strategy for the synthesis of chloromethylated polystyrene (CMPS) based on nucleophilic substitution and Friedel–Crafts alkylation.[109] The OH-rich functionalized polystyrene was further modified using cyanuric chloride (CC), DCX, 4,4′-bis(chloromethyl)-1,1′-diphenyl (BCMBP), and formaldehyde dimethyl acetal (FDA) as cross-linking agents, based on the Friedel–Crafts alkylation reaction, yielding a polymer with a hierarchical porous structure. The polystyrene-based HCPs exhibited a high SSA (601 m^2 g^{-1}) and oxygen content of 13.04 wt% which showed good adsorption properties for aniline in aqueous solution, especially rapid diffusion of aniline in kinetic adsorption. This general synthetic scheme was important for the preparation of other functionalized HCPs.

Heterocyclic compounds are frequently utilized as monomers in the construction of HCPs because of their unique

Table 2 HCPs constructed with different crosslinkers

No.	HCP	Monomers	Cross linker	Solvent	S_{BET} (m^2 g^{-1})	V_{total} (cm^3 g^{-1})	Applications	Ref.
1	HMP-2	Carbazole	BCMBP	DCE	565	0.458	CO_2 capture	106
2	Bn-CD-HCP	β-Cyclodextrin	BCMBP	DCE	1107	—	Albendazole uptake	107
3	PPN	Triphenylamine	DBX	DCE	1165	1.033	Hydrogenation catalyst	108
4	HCLPs	PS@DBP-DCX	DCX	o-DCB	601	0.539	Water treatment	109
5	HCP	Benzimidazole	DCX DBX	DCE	1063	1.03	CO_2 capture and conversion	110
6	HCPs	Benzylimidazole salts	DCX DBX	DCE	1017	1.63	CO_2 capture	111
7	HPP	Tetraphenylethene and DPT	DCX	DCE	1230	1.03	Dye adsorption and supercapacitor	112
8	HCPs	Benzene	DMB	DCE	442	—	Photocatalytic	113
9	Py-DMB HCP	Pyrrole	DMB	Nitrobenzene	137	0.123	Solid-phase extraction	114
10	DB18C6-HCP	Dibenzo-18-crown-6	DMB	Nitrobenzene	530	0.32	Gold adsorption	115
11	HCPB	Benzene	DMB	Nitrobenzene	593	0.38	Lithium-ion batteries	116
12	MIHCPs	Naphthalene and 3,5-dinitrosalicylic acid	DMB	Nitrobenzene	1134	—	Fluorescently determined	117

o-DCB was *o*-dichlorobenzene, DPT was 4-(5,6-diphenyl-1*H*-benzimidazol-2-yl)-triphenylamine.

structures. Ali Enis Sadak synthesized microporous HCPs using 4,4′-bis(N-carbazolyl)-1,1′-biphenyl, a monomer containing a bicarbazole unit, and various structural cross-linkers, including formaldehyde dimethyl acetal (FDA), p-dimethoxybenzene, and cyanuric chloride (Fig. 4a).[78] All HCPs exhibited an SSA exceeding 500 m^2 g^{-1} and an ultra-microporous pore size of 0.57 nm. Typically, the YBN-DMB, cross-linked by DMB, showed the highest SSA (968 m^2 g^{-1}) and microporous pore volume (0.46 cm^3 g^{-1}).

Subsequently, they conducted similar research using N,N,N′,N′-tetraphenyl-1,4-phenylenediamine as monomer.[118] Liang et al. crosslinked and extended the aromatic skeleton of conjugated microporous polymers (CMPs) using methylene bonding with different cross-linking agents, achieving an impressive specific surface area of 2267 m^2 g^{-1}.[26] This post-braiding method reconfigured the porous skeleton of CMPs, leading to a substantial increase in CO$_2$ uptake.

DCX, BCMBP and DMB are frequently employed as cross-linkers to modulate the microstructure of hyper-crosslinked polymers; e.g. Ji et al. utilized FDA, DCX, and BCMBP as cross-linkers to prepare starch-graft-styrene hypercrosslinked polymers (SSHCPs) through a Friedel–Crafts alkylation reaction catalyzed by FeCl$_3$, using starch-graft-styrene copolymer as monomer (Fig. 4b).[58] Among the products, SSHCP-3, which employed BCMBP as the cross-linker, exhibited the highest SSA (818 m^2 g^{-1}). The SSA of SSHCPs increased with the number of aromatic rings in the cross-linker. However, the HCPs exhibited abundant microporous structures regardless of the cross-linker. Additionally, when used as the simplest aromatic monomers with DMB as the cross-linking agent, benzene and naphthalene could construct HCPs with a high SSA, typically around 500 m^2 g^{-1}, with slight variations in pore size distribution depending on the reaction conditions.[113] HCPs cross-linked by carbonized DMB demonstrate an excellent electrochemical performance in energy storage.[116,119] Moreover, Chen et al. introduced 3,5-dinitrosalicylic acid as a co-crosslinker in the naphthalene–DMB system, producing HCPs with an SSA of 1134 m^2 g^{-1} and pore sizes ranging of 5–8.5 Å.[117]

Heterocyclic compounds could also be utilized to prepare HCPs via cross-linking reactions with DMB. Wu et al. synthesized Py-DMB HCP using pyrrole as monomer and p-dimethoxybenzene as cross-linker. Unlike other HCPs, this novel heterocyclic polymer exhibited a low SSA (137 m^2 g^{-1}) while demonstrating hydrogen bonding and π–π stacking abilities during the adsorption.[114] Py-DMB HCP exhibited an excellent performance for the solid-phase extraction of phenylurea herbicides. The application of HCPs constructed with DMB as cross-linker was notably broad. By using dibenzo-18-crown-6 and dibenzo-24-crown-8 as monomers, multi-microporous HCPs were synthesized with a microporous SSA exceeding 320 m^2 g^{-1} and pore sizes predominantly distributed between 0.5–2.1 nm.[115] B18C6-HCP demonstrated a high adsorption capacity for gold (1667 mg g^{-1}), indicating that porous organic polymers hold significant potential for development in noble metal adsorption.

In addition to the commonly used cross-linking agents novel agents for polymerization had been increasingly reported. Dai et al. synthesized fluorinated porous organic networks (F-PONs) with a high fluorine content and robust nanoporous structure using perfluorinated benzylic alcohols as cross-linking agents and polydivinylbenzene (PDVB) monomer. The F-PONs exhibited a high fluorine content (22 at%), large SSA (771 m^2 g^{-1}), and notable chemical and thermal stability.[121] This straightforward method could be further extended to rigid aromatic monomers for the preparation of fluorinated HCPs. Furthermore, Tan's group was actively developing new types of cross-linking agent.[120] As shown in Fig. 5, they utilized 1,3,5-benzenetricarbonyl trichloride (BTC) as cross-linking agent to weave pyrene (Py) components to prepare HCP (HMPNs). The polymer showed a uniform spherical morphology with a size range of approximately 200 nm and SSA of 668 m^2 g^{-1}. This material had prospects in the field of biomedical applications.

It was evident that the microstructure of HCPs could be further regulated through the selection of cross-linking agents. Therefore, the development of new cross-linking agents remained a persistent pursuit.
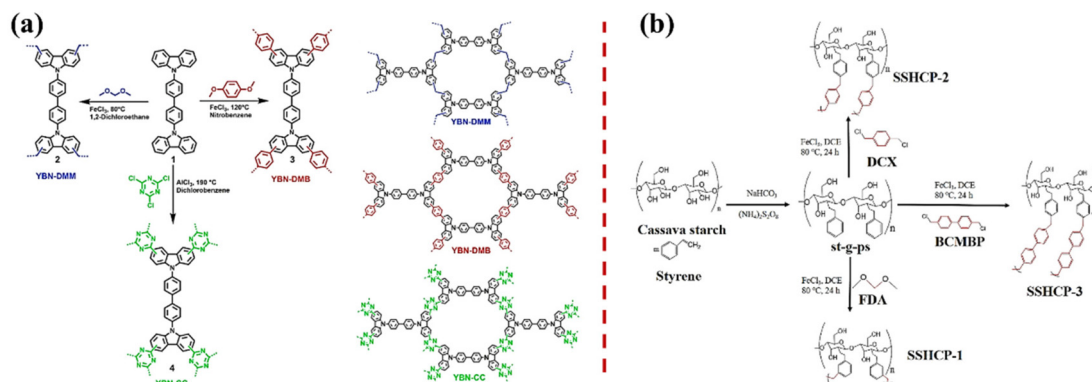

Fig. 4 (a) Synthesis of three microporous polymers by using dicarbazole building blocks with different crosslinkers.[78] Copyright 2020, Elsevier. (b) Synthetic strategy of SSHCPs with some typical external crosslinkers containing biphenyl, methylene, and xylene, respectively.[58] Copyright 2021, Elsevier.

© 2025 The Author(s). Published by the Royal Society of Chemistry
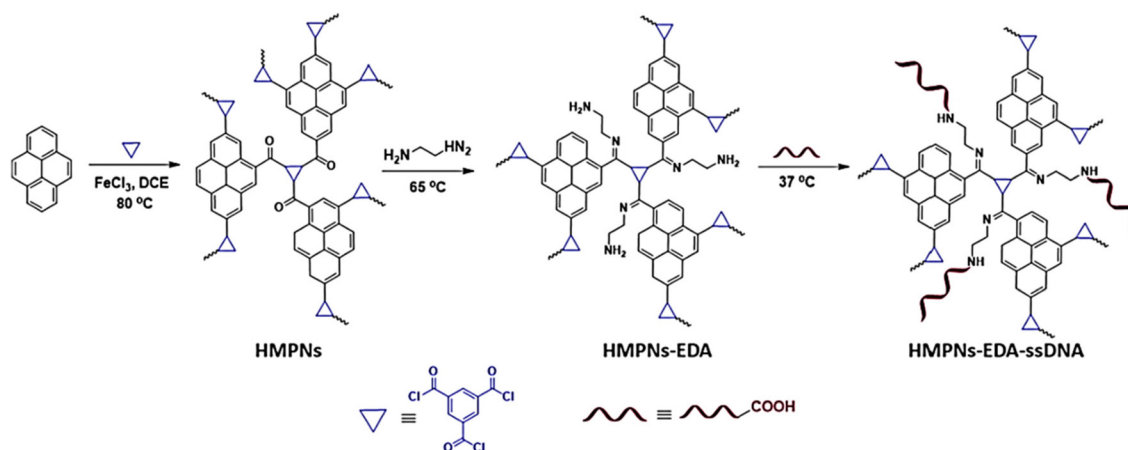
RSC Appl. Polym., 2025, 3, 746–766 | 753

Fig. 5 Synthesis of hypercrosslinked microporous polymer nanospheres (HMPNs) based on a Friedel–Crafts reaction by using pyrene as monomer and 1,3,5-benzenetricarbonyl trichloride as crosslinker.[120] Copyright 2022, Elsevier.

3.1.3 Reaction conditions. HCPs synthesized under varying conditions experienced significant changes in the microstructure, which effectively altered the SSA of the material. Tuning the monomer often led to changes in both the SSA and pore structure of the HCPs.

Some research on the effect of the ratio of crosslinker to monomer has been reported. Jeřábek et al. prepared mesoporous poly(divinylbenzene) at monomer and solvent ratios of 1 : 5 and 1 : 10 which exhibited exceptionally high specific surface areas (934–975 m^2 g^{-1}) in both the expanded and dried states, without micropores, and displayed unprecedented porosity.[122] Meanwhile, Gilani et al. synthesized HCPs based on polystyrene by varying the ratio of cross-linker to monomer (1–5) and the reaction time.[80] Through optimization, the SSA of the HCPs reached the maximum of 823 m^2 g^{-1} when the synthesis time was 13 h and the cross-linker-to-monomer ratio was 3.

Cooper et al. prepared HCPs using DCX and BCMBP as cross-linking agents by adjusting the ratios of different monomers and the reaction conditions to control the pore structure of the polymers.[123] It was found that, at a DCX-to-BCMBP ratio of 1 : 3, the as-prepared HCPs exhibited a high methane adsorption capacity of up to 5.2 mmol g^{-1} at 20 bar and 298 K. This finding indicated that adjusting the reactant ratios allowed for the regulation of the polymer's microstructure, offering a new approach for optimizing the pore structure of HCPs.

When formaldehyde dimethyl acetal (FDA) was used as cross-linking agent, increasing the ratio of 1,3,5-triphenylbenzene (TPB) to L-tyrosine (L-Tyr) monomers led to a gradual increase in the SSA of the HCPs.[97] Bai et al. conducted similar research by adjusting the molar ratio of 1-(benzyloxy)-4-ethylbenzene (BP-AO) to diphenyl. When the molar ratio was 1 : 0 (BP-AO : diphenyl), the SSA reached 948 m^2 g^{-1}, and a mesoporous structure was observed.[82] However, when the ratio decreased to 1 : 3 (BP-AO : diphenyl), the specific surface area decreased to 246 m^2 g^{-1}. This demonstrated that the method

was an effective strategy for regulating both the specific surface area and pore structure of HCPs.

Additionally, when phenothiazine, a monomer with a π-electron conjugated structure containing nitrogen and sulfur atoms—was cross-linked with FDA, the highest specific surface area of the HCP (209 m^2 g^{-1}) was obtained at the ratio of 1 : 4 (phenothiazine : FDA).[57] Structural characterization results illustrated that the increase in the amount of FDA also led to a higher number of residual methoxy groups, which decreased the degree of cross-linking of the HCPs. This phenomenon directly resulted in changes in the micropore size.

Fierro et al. used anthracene (A), benzene (B), carbazole (C), or dibenzothiophene (D) as monomers to tune the microstructure of HCPs. When carbazole was used as monomer, the specific surface area and micropore volume were the highest (1132 m^2 g^{-1}, 0.34 cm^3 g^{-1}) at a monomer : catalyst : crosslinker ratio of 1 : 1 : 2.[93] Both carbazole- and dibenzothiophene-based HCPs displayed type Ib adsorption–desorption isotherms curves, indicating the well-developed microporous structures. For the anthracene-derived HCP sample, the microporous structure was the most developed (67%) at a ratio of 1 : 1 : 2 (C : $FeCl_3$: FDA). Therefore, optimizing the reaction conditions for HCPs could effectively enhance the SSA and pore structure of HCPs.

Furthermore, Zou et al. systematically investigated the effects of synthesis conditions on the porosity of HCPs.[40] Using 9-phenylcarbazole as the monomer and formaldehyde dimethyl acetal (FDA) as the cross-linker, they prepared a series of HCPs by varying the molar ratio of cross-linker to monomer, reaction temperature, amount of catalyst, and concentrations of reactants. The results indicated that the molar ratio of cross-linker to monomer was the primary factor affecting the SSA. Increasing the reaction temperature or altering the amount of catalyst significantly increased the total pore volume of HCPs at the expense of some SSA. Further adjustment of the reactant concentration could achieve both a high SSA and pore volume, resulting in an HCP with an SSA as

high as 769 m^2 g^{-1} and a pore volume of 1.27 cm^3 g^{-1}. Similarly, Bisio *et al.*[124] regulated the structure of HCPs by adjusting the ratio of tetraphenylmethane (TPM) to FDA. The polymer still has a high specific surface area and pore volume. As the amount of FDA increased, the specific surface area of the HCPs increased. When the TPM/FDA ratio was 1/30, the specific surface area of mPAF reached the maximum (1318 m^2 g^{-1}), further indicating that the ratio of monomers and cross-linkers could regulate the SSA of HCPs. In addition, mPAF-1/16 showed a good adsorption performance for toluene adsorption, which was attributed to the swelling effect of the polymer network that reduced the adsorption performance of the highly cross-linked polymer.

3.2 Heteroatomic groups of HCPs

The chemical structure of HCPs could generally be regulated by incorporating specific elements or using monomers with functional groups. HCPs containing various functional groups or heteroatoms enhanced the structural diversity of HCPs. Moreover, the porous structure was maintained, which led to an exceptional performance in practical applications.

3.2.1 Construction of HCPs with N-containing functional groups. Functionalization was commonly employed to regulate the chemical structure of HCPs. Zhang *et al.* prepared HCPs using α,α′-dichloro-*p*-xylene (DCX) as monomer and 1,2-dichloroethane (DCE) as solvent catalyzed by FeCl$_3$.[125] They also synthesized nitrogen-doped HCPs (HCP-N) by copolymerizing 1-benzylimidazole with DCX. The SSA of HCP and HCP-N were 939 m^2 g^{-1} and 612 m^2 g^{-1}, respectively, both exhibiting hierarchical porous structures.

Liu *et al.* synthesized a series of novel layered porous N-rich heterocyclic hypercrosslinked polymeric composite materials (PCMOPs) containing carbazole and phthalazinone groups using DCPHPZ and DCDPHPZ, two rigid and twisted compounds, as monomers through mild and facile cross-coupling and self-coupling reactions (Fig. 6a).[73] The HCPs prepared *via* cross-coupling exhibited a higher BET SSA (675 m^2 g^{-1}) and pore volume (0.49 cm^3 g^{-1}). Recently, Tan's group used three

different complex compounds, 9-fluorenylmethyl pentafluorophenyl carbonate (FPC), 9-fluorenylmethyl 1-benzotriazolyl carbonate (FBC) and 9-fluorenylmethyl succinimidyl carbonate (FSC), as monomers to prepare polymers rich in nitrogen atoms, carbonyl groups and ester groups through cross-coupling in CH$_2$Cl$_2$, achieving the highest BET surface area of 1367 m^2 g^{-1}.[127] These results indicated that fine-tuning the molecular structure of the monomer building blocks allowed for the adjustment of the structural properties of the resulting polymers. Additionally, Li *et al.* synthesized PTPIM and PTPIM-IL with polymer network structures through Friedel–Crafts alkylation reactions, using novel triazine-linked triphenylimidazole (TPIM) and triphenylimidazolium (TPIM-IL) as monomers, respectively.[126] Due to the branched, bulky, and rigid heterocyclic structures of the monomers, the resulting PTPIM and PTPIM-IL networks exhibited a relatively high SSA of 982 m^2 g^{-1} and 570 m^2 g^{-1}, respectively (Fig. 6b).

Functionalized HCPs could be synthesized using phenyl monomers substituted with specific functional groups.[95] The HCPs prepared with chlorobenzyl-substituted benzene had an SSA of up to 1249 m^2 g^{-1}. Further functionalization with ethylenediamine yields –NH$_2$-modified HCPs, with a nitrogen content reaching up to 25.7 wt% and SSA of up to 1115 m^2 g^{-1}. The –NH$_2$– substituted monomer, due to its abundant affinity sites, was commonly utilized in the development of new types of iodine-adsorbing HCP. As shown in Fig. 7, two types of aniline-based HCP (AHCPs), AHCP-1 and AHCP-2, were synthesized using aniline as monomer through Friedel–Crafts alkylation and Scholl reactions, which exhibited high chemical and thermal stability. Additionally, the presence of substituents introduced significant steric hindrance on the phenyl ring, resulting in a much smaller SSA for AHCP (14 m^2 g^{-1}) compared with the unsubstituted monomer benzene. This result can be traced back to the report of the Cooper group, who prepared HCPs from benzene and aniline as monomers, and significantly reduced the SSA (7 m^2 g^{-1}, 100% aniline) of HCPs by increasing the aniline content.[42] The increased of the aniline content led to enhanced CO$_2$/N$_2$ selectivity.
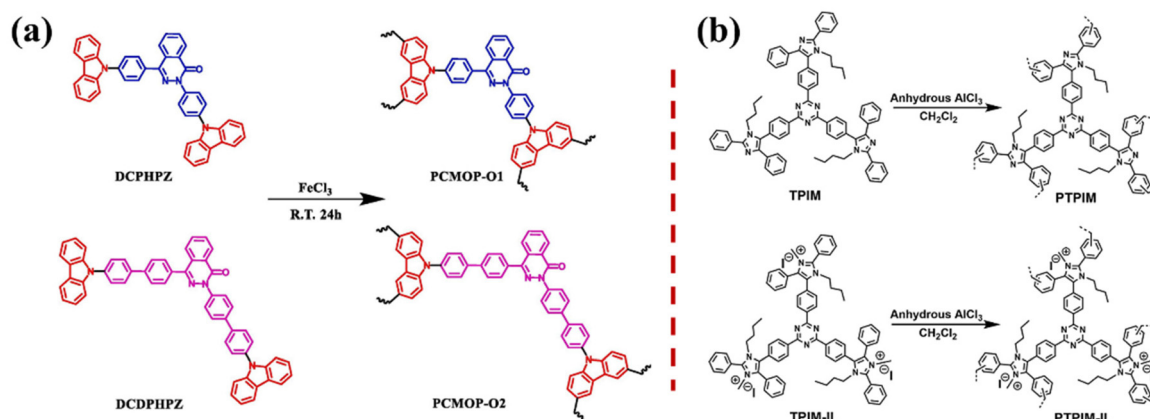

Fig. 6 (a) Synthesis of carbazole- and phthalazinone-based porous organic polymers.[73] Copyright 2020, Elsevier. (b) Synthesis of triazine-containing poly(triphenylimidazole) (PTPIM) and poly(triphenylimidazolium) (PTPIM-IL).[126] Copyright 2023, Elsevier.
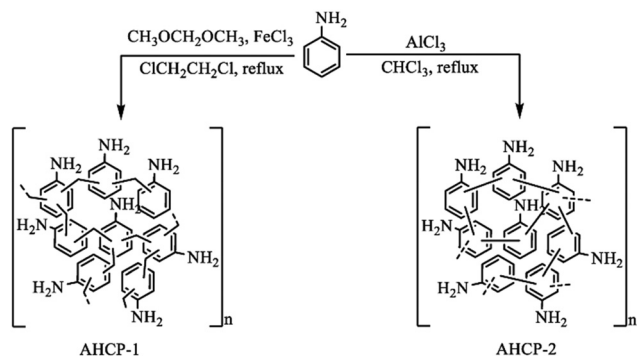
© 2025 The Author(s). Published by the Royal Society of Chemistry

RSC Appl. Polym., 2025, **3**, 746–766 | **755**

Fig. 7 Synthesis of aniline-based hypercrosslinked polymers.[128] Copyright 2023, Multidisciplinary Digital Publishing Institute (MDPI).

Nevertheless, the functionalized HCPs demonstrated effective iodine capture in both the aqueous and gaseous phases. AHCP-1 showed high static iodine adsorption (250 wt%) in aqueous solution, while AHCP-2 had an excellent iodine capture rate (596 wt%) in vapor adsorption.[128]

Different functional groups containing nitrogen were employed to regulate the structure of HCPs. Li *et al.* constructed HCPs from nitrogen-containing monomers (bis(*N*-pyrrolyl)-1,2,4,5-tetrazine (TPy), bis(*N*-indolyl)-1,2,4,5-tetrazine (TIn), and bis(*N*-carbazolyl)-1,2,4,5-tetrazine (TCz)) over various catalysts (FeCl$_3$, CF$_3$SO$_3$H and AlCl$_3$).[129] Further studies demonstrated that the SSA of HCPs could be adjusted not only by varying the length of rigid linkers but also by altering the size of the reactive motifs. Moreover, HCPs with

diverse pore structures could be constructed using various N-heterocyclic monomers, allowing effective regulation of nitrogen content.[87] Pan *et al.* synthesized TZ-HCP1D with a high SSA of 1139 m^2 g^{-1}, by cross-linking modified 3,6-di (pyridin-2-yl)-1,2,4,5-tetrazine (pytz) and benzene or 9*H*-fluorene using FDA as cross-linker.[91] The high SSA, coexistence of micro- and mesopores and modification with specific groups (–N=N–) improved the accessibility of photocatalytic active sites and facilitated molecular transport. Similarly, Das *et al.* reported trisbiphenylene-based HCP (TBHCP-OH) containing CO$_2$-philic groups (–N=N and –OH) for CO$_2$ adsorption.[59] The polymer featured a rich mesoporous structure (235 m^2 g^{-1}) and functional groups, demonstrating effective adsorption performance.

3.2.2 Preparation of HCPs with O-containing functional groups. Monomers or crosslinkers with oxygen-containing functional groups were crucial for constructing porous polymer networks, particularly for HCPs used for CO$_2$ and H$_2$ adsorption.[12] Building on this, the Tan group synthesized HCPs through self-crosslinking of the monohydroxy compound benzyl alcohol (BA) and dihydroxymethyl monomer 1,4-benzenedimethanol (BDM) with a high SSA (>700 m^2 g^{-1}) and pore structures ranging from micropores to macropores (Fig. 8a).[130]

Han *et al.* prepared hypercrosslinked polymer (TA-HCP) by utilizing tannic acid, a biomolecule rich in –OH groups, as the raw material.[131] The resulting polymer achieved an SSA of 610 m^2 g^{-1}. The hydroxyl groups in TA-HCP served as active sites for subsequent vanadium functionalization, leading to the preparation of the catalyst TA-HCP-VO which demonstrated excellent performance in the oxidation of thioethers.
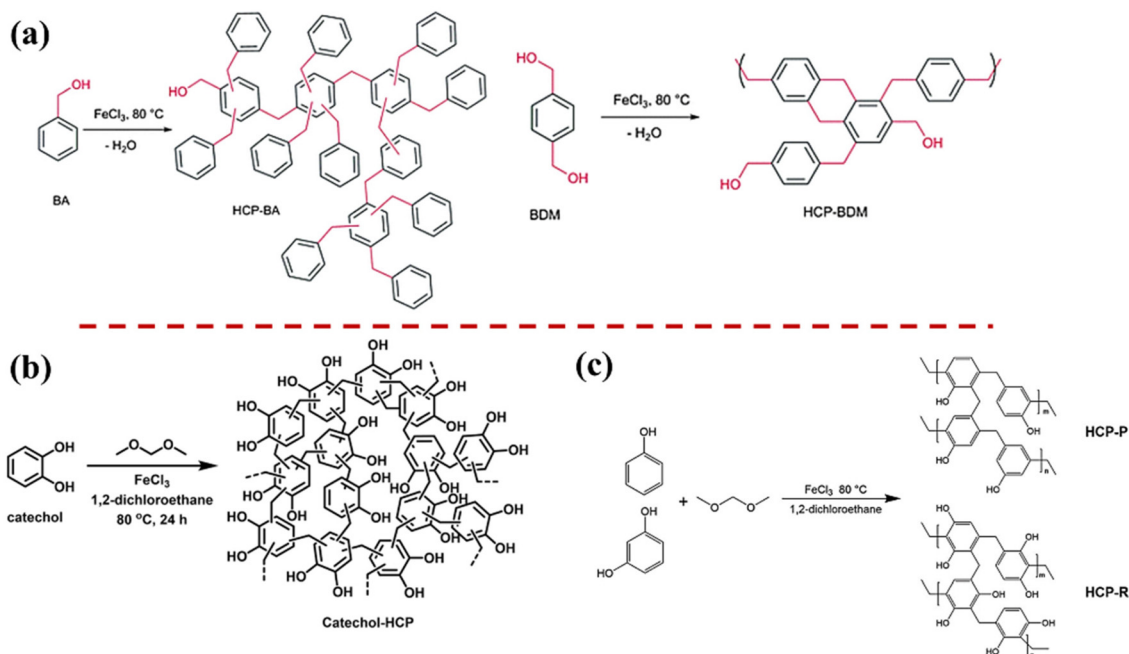

Fig. 8 (a) Synthesis of HCP–BA and HCP–BDM based on a Friedel–Crafts alkylation reaction catalyzed self-condensation.[130] Copyright 2013, The Royal Society of Chemistry. (b) The scheme of catechol-based HCP.[53] Copyright 2020, Springer. (c) Fabrication of hypercrosslinked hydroxyl-rich polymer (HCP-P and HCP-R).[56] Copyright 2020, Elsevier.

© 2025 The Author(s). Published by the Royal Society of Chemistry

Moreover, aromatics with the hydroxyl groups at various substitution sites could effectively regulate the chemical structure. As demonstrated in Fig. 8b, Thanchanok synthesized HCPs rich in hydroxyl groups using phenol, hydroquinone, and catechol as monomers.[53] Different from those constructed with unsubstituted monomers, the HCPs, enriched with hydroxyl groups, exhibited an SSA of less than 50 m^2 g^{-1}. Similarly, Liu *et al.* prepared two types of hypercrosslinked hydroxyl-rich polymer, HCP-P and HCP-R, using phenol and catechol as raw materials, achieving specific surface areas of 183 m^2 g^{-1} and 77 m^2 g^{-1}, respectively.[56] These polymers were rich in mesopores and macropores, with HCP-P demonstrating a particularly abundant mesoporous structure (Fig. 8c).

HCPs rich in hydroxyl groups were frequently utilized for water pollutant treatment (Fig. 9a and b). Tian *et al.* designed two types of HCP using Bisphenol A and Fluorene-9-bisphenol as monomers through phosphorylation with phosphorus oxychloride, for uranium adsorption. The functionalized PHCP-2 (564 m^2 g^{-1}) exhibited a slightly lower SSA than HCP-2 (663 m^2 g^{-1}), with pore sizes predominantly distributed between 2.2 and 2.8 nm.[72] Subsequently, they employed various functionalization methods to modify the HCP from Fluorene-9-bisphenol monomer, which had an SSA of 640 m^2 g^{-1}.[70] Specifically, they synthesized a functionalized adsorbent (HCP-AO, SSA of 58 m^2 g^{-1}) *via* aminooximation using chloroacetonitrile-modified HCPs. The decrease in SSA was attributed to the grafting of a substantial number of new groups within the HCPs, which occupied the pore space, consequently reducing the SSA and pore volume of the material.[132]

Moreover, by utilizing hydroxyl-rich and highly aromatic compounds as monomers, the resulting porous polymers demonstrated excellent physicochemical properties and a dis-tinct structural morphology, which were influenced by the cross-linking sites.[66] As illustrated in Fig. 10a, under the cross-linking of formaldehyde dimethyl acetal (FDA) and two hydroxyl-containing monomers, *meso*-hydrobenzoin (MHB) and 1,1,2,2-tetraphenyl-1,2-ethanediol (TPED), HCPs with hierarchical porous structures (552 m^2 g^{-1}, 0.496 cm^3 g^{-1}) and nanofiber morphologies (HPOP-3) could be formed. This material was particularly advantageous for the rapid adsorption of pharmaceutical and personal care product (PPCP) molecules. The synthesis of polymers from natural oxygen-containing aromatic phenolic compounds derived from biorefinery waste represented a green and sustainable approach. Chen *et al.* prepared various oxygen-rich HCPs from the liquid products of lignin depolymerization *via* Friedel–Crafts alkylation.[60] The HCPs exhibited an SSA ranging from 14 to 247 m^2 g^{-1} and oxygen contents between 18 and 31 wt%. Further analysis indicated that pore size distribution and the presence of oxygen-containing functional groups were crucial in determining the adsorption performance.

In addition to, methoxy groups can also be employed as modifying agents. Huang *et al.* synthesized hypercrosslinked resin (HCLP) using chloromethylated polystyrene (CMPS) modified with anisole as monomer (PS-AI) and FDA as cross-linking agent.[71] The polymer showed a high SSA and abundant methoxy groups (Fig. 10b). The functionalized resin monomer PS-AI contained strong electron-withdrawing groups (–OCH$_3$), resulting in a specific surface area of only 73 m^2 g^{-1}. Upon further crosslinking, the specific surface area increased to 650 m^2 g^{-1}. The presence of basic groups (–OCH$_3$) in the anisole enabled the formation of hydrogen bonds with aniline, rendering this HCLR particularly effective for aniline adsorption in aqueous solutions. Chen *et al.* prepared HCPs by select-
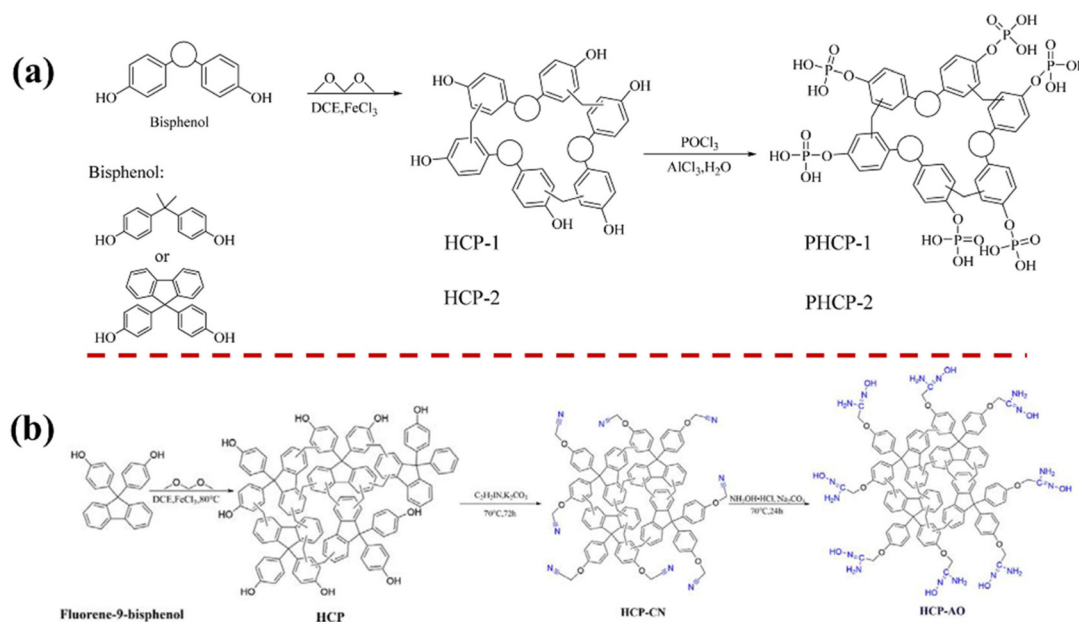

Fig. 9 (a) Synthesis of Bisphenol A- and Fluorene-9-bisphenol-based HCPs.[72] Copyright 2021, Elsevier. (b) Synthesis of Fluorene-9-bisphenol-based HCPs and further functionalization.[70] Copyright 2023, Elsevier.

© 2025 The Author(s). Published by the Royal Society of Chemistry

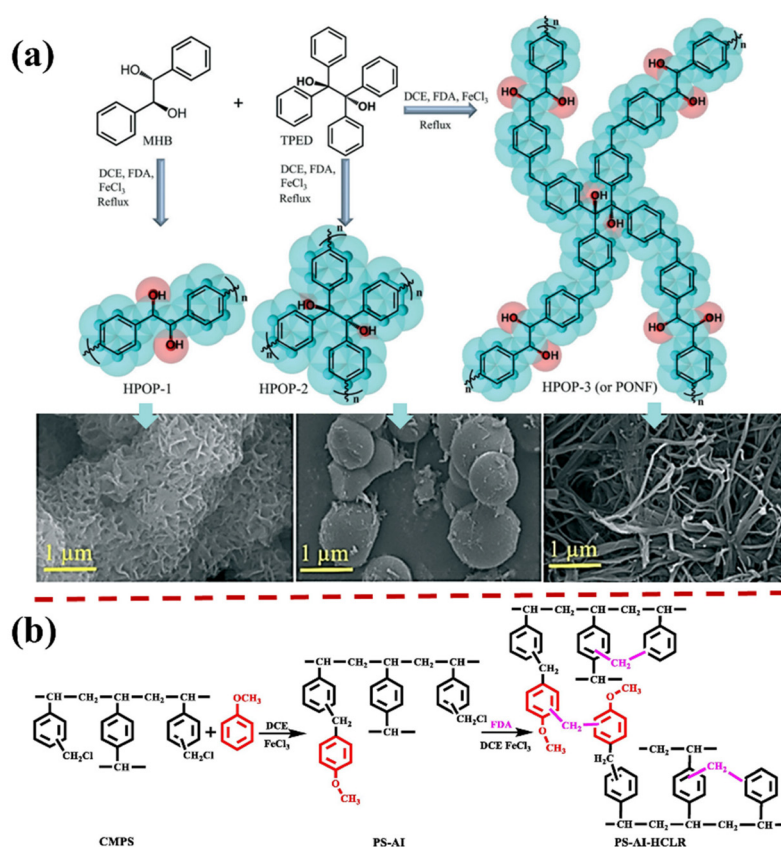*RSC Appl. Polym.*, 2025, **3**, 746–766 | **757**

Fig. 10 (a) Schematic of MHB- and TPED-based HCPs and different surface morphology.[66] Copyright 2022, The Royal Society of Chemistry. (b) Synthetic procedure of anisole-modified hyper-cross-linked resins.[71] Copyright 2020, Elsevier.

ing phenols with methoxy and hydroxyl groups substituted at different positions as monomers, which effectively regulated the SSA (14–247 m^2 g^{-1}), pore structure, oxygen content (18.5–30.7 wt%), and oxygen-containing functional groups (methoxy and hydroxyl).[60] Optimized pore size, electron cloud density, and chemical group distribution were crucial for CO_2 and iodine adsorption.

Modification strategies preserved the specific functional group structure and the SSA of polymers, thereby enabling the multifunctionalization of HCPs. This approach was relatively simple which effectively introduced specific elements into the HCP system, contributing to its widespread application. However, this method typically required multiple steps, which posed challenges in practical operation.

3.2.3 Preparation of HCPs with other heteroatomic-containing functional groups. Heteroatoms could be introduced through post-modification of HCPs constructed from condensed aromatic rings. For instance, Nikoshvili *et al.* synthesized HCPs with –SO$_3$H and –NO$_2$ groups using naphthalene and 1-naphthol as monomers, to explore the impact of the functional groups on the porosity of the polymer.[149] The samples exhibited reduced SSA, and the pore structure shifted towards mesopores and macropores. Meanwhile, Beyzavi *et al.* prepared a coal tar crosslinked polymer (CTHP) using coal tar as an aromatic monomer *via* self-condensation, and sub-

sequently synthesized sulfur-modified HCP (CTHP-SES) based on CTHP through a post-modification strategy. The SSA decreased from 828 m^2 g^{-1} to 212 m^2 g^{-1} after modification.[133]

Post-modification involved secondary chemical reactions on the network which expanded the range of functional group options, thereby broadening the applications of HCPs. Ghaemi *et al.* synthesized a chlorobenzyl hypercrosslinked adsorbent (B-Cl) for CO_2 adsorption *via* a Friedel–Crafts alkylation reaction.[95] They adopted a low-cost impregnation strategy followed by functionalization with ethylenediamine (EDA) in the presence of water (B-Cl-1) and methanol (B-Cl-2). The SSA of the functionalized HCPs (B-Cl-2, 409 m^2 g^{-1}) was significantly lower (B-Cl, 1249 m^2 g^{-1}, before functionalization), likely due to the obstruction of amine substances within the adsorbent voids, thereby reducing the adsorption capacity. Similarly, Yang *et al.* constructed HCPs using 1,1,1-trimethyl-3,3,3-triphenyldisiloxane (TTD) as monomer and FDA as crosslinking agent based on previous work.[89,96] At the ratio of 1 : 4.5 (TTD : FDA), the specific surface area of the as-prepared HCP (HCP-TTD-3) approached 1300 m^2 g^{-1}. The microporous structure significantly enhanced the adsorption performance of the material. Furthermore, functionalization of the HCP was achieved by condensing with 3-(2-aminoethylamino)propyl-dimethoxymethylsilane (AAMD). The introduction of Si–O functional groups into the HCP structure led to an excellent

adsorption performance for chromium ions, with an adsorption capacity as high as 76.9 mg g^{-1}, surpassing the previously reported adsorbents. During functionalization, the reaction between AAMD and Si–OH, coupled with the dehydration condensation between Si–OH groups, formed new Si–O–Si bonds, thereby generating new pore structures, with pore sizes concentrated in the ranges of 0.4–0.8 nm and 1–2 nm. Additionally, the introduction of functional groups, which occupied part of the pore volume of the HCP, resulted in a decreased SSA.

3.3 Morphological regulation of HCPs

HCPs, as porous polymers, have emerged as an excellent support for nanoscale separation and active substance loading. Various methods are employed to regulate the morphology of HCPs. By utilizing silica nanoparticles as templates, Tan *et al.* prepared hollow microporous nanorods (SiO$_2$@PS-DVB) using a mixture of polystyrene and divinylbenzene, significantly expanding the morphological structure of the polymer.[136] Qiao *et al.* synthesized HCP films with hierarchical porosity through an *in situ* cross-linking strategy (Fig. 11a).[134] They cross-linked diblock copolymer micelles of poly(ethylene oxide)-b-polystyrene (PEO-b-PS) *via* the Friedel–Crafts reaction. By adjusting the self-assembly structure of PEO-b-PS, uniform HCP hollow spheres with an SSA of up to 1123 m^2 g^{-1} were generated.

Additionally, the pore size of HCPs could be effectively modulated by varying the length of the PEO segments. The encapsulation of Pd nanoparticles within hypercrosslinked polymer hollow spheres exhibited excellent catalytic activity in the oxidation of aromatics and aliphatic alcohols. As shown in Fig. 11b, Kim *et al.* synthesized polymer nanosheets without templates or surfactants *via* Lewis acid (FeCl$_3$)-catalyzed Friedel–Crafts alkylation-induced crosslinking using a series of functionalized aromatic compounds as monomers.[135] Mechanistic studies revealed that the byproducts generated during the reaction coordinated the interaction between the catalyst (acid) and monomer (base), thereby driving self-assembly in a one-pot condensation. Notably, based on the study of the structural evolution and formation mechanism of HCPs, a non-metallic method for constructing hypercrosslinked hollow spherical polymers was also developed. Zhang *et al.* prepared hypercrosslinked tubular polymer nanofibers (TPNF) by adding polydimethylsiloxane to DCE solution containing dichlorodiphenylmethane.[137] Tubular carbon nanofibers were subsequently prepared by carbonization. The SSA of TPNF decreased with increasing of the carbonization temperature, reaching up to 423 m^2 g^{-1} (TCNF at 650 °C). This material could serve as an efficient, lightweight absorbent with significant potential application in the field of wave absorption. As shown in Fig. 11c, Patra *et al.* synthesized tris-metallocene hypercrosslinked porous polymers. Morphological transition
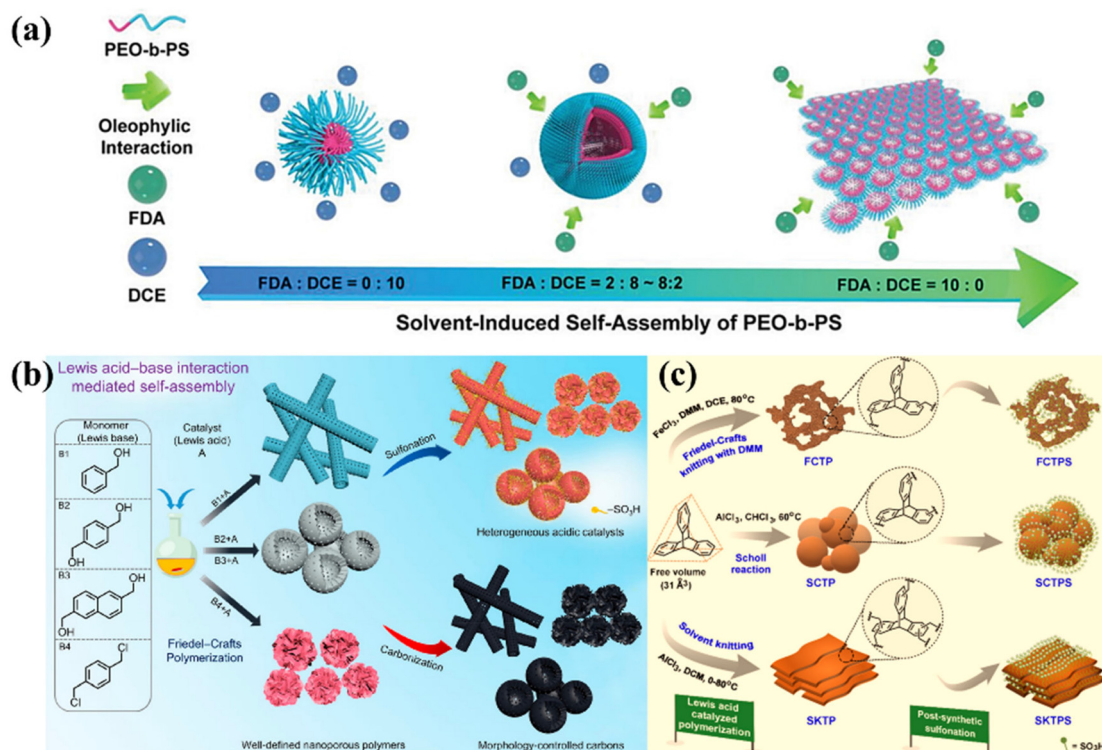

Fig. 11 (a) Solvent-induced self-assembly strategy to produce PEO-b-PS-based porous polymers.[134] Copyright 2019, Wiley-VCH. (b) Synthesis processes of hierarchical nanoporous polymers *via* the Friedel–Crafts reaction polycondensation.[135] Copyright 2019, American Chemical Society. (c) Synthesis of SCTPS through a Scholl reaction using chloroform at 60 °C for 24 h.[47] Copyright 2022, American Chemical Society.
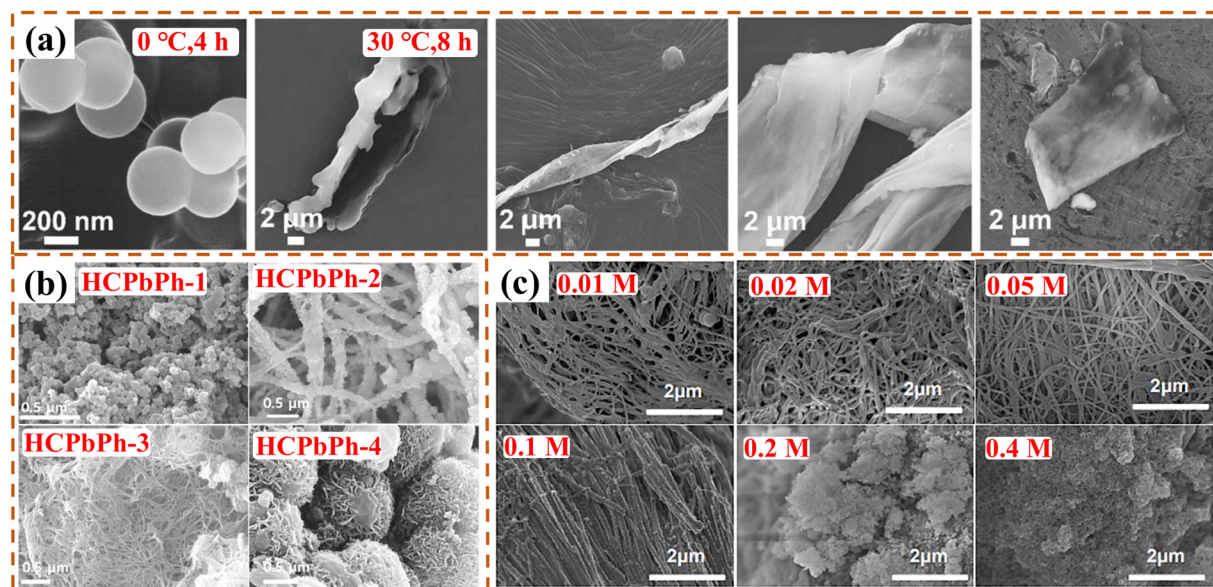
Fig. 12 (a) Solvent knitting of a 2D nanosheet polymer: The morphology at the initial stage of the reaction was nanospheres; the nanospheres fused into nanoribbons; finally, the nanoribbons start to assemble with the increase of solvent knitting temperature and time to form 2D nanosheets.[47] Copyright 2022, American Chemical Society. (b) Morphological diversity: the polymers synthesized with different monomer/cross-linker ratios (named as HCPbPh-1 *etc.*).[45] Copyright 2021, Elsevier. (c) Surface morphology of benzene-based hypercrosslinked porous polymers with different monomer concentrations.[100] Copyright 2017, American Chemical Society.

from irregular aggregates (FCTP) to rigid spheres (SCTP) and subsequently to two-dimensional nanosheets (SKTP) was observed.[47] The results indicated that reaction temperature, catalyst, and solvent played important roles in determining the morphology. Combined mechanical, microscopic, and computational studies suggested that the evolution of two-dimensional nanosheets of highly porous solvent-woven polymers (SKTP, 2385 m^2 g^{-1}) resulted from the sequential hierarchical self-assembly of nanospheres and nanobelts. The directional growth of tris-metallocene HCPs from irregular aggregation to rigid spheres, and subsequently to two-dimensional nanosheets, was tunable *via* Friedel–Crafts weaving, Scholl reaction, and solvent weaving (Fig. 12a), offering valuable insights for the design of functionalized HCPs for specific applications.

Morphology modulation of HCPs by reaction conditions has been frequently reported. By adjusting the ratio of monomers to crosslinkers or the reaction time, the SSA and morphologies of HCPs could be controlled.[100,135,138] As shown in Fig. 12b, Kim *et al.* constructed well-porous polymer particles *via* crosslinking-induced self-assembly by tuning the ratio of biphenyl (bPh) to formaldehyde dimethyl acetal (FDA) without using any templates or surfactants.[45] At a bPh to FDA ratio of 1:4, the sample with a nanoflower structure exhibited the largest SSA (1100 m^2 g^{-1}). At bPh:FDA ratios of 1:2 or 1:3, the morphology appeared as polymer fibers. Reducing the ratio to 1:1 (bPh:FDA) resulted in amorphous nanospheres with an SSA of only 101 m^2 g^{-1}. Therefore, in the system where FDA acted as the crosslinker, the morphological properties of the polymers in solution largely depended on the concentration of FDA. By coordinating the active sites of FDA with

aromatic compounds, the microstructure could be effectively regulated (Fig. 12c).[100]

4   Application of HCPs

The porous structure of HCPs facilitated their extensive application in diverse fields, including gas adsorption and separation, pollutant treatment, catalysis, and energy storage.

4.1   Gas adsorption

HCPs have predominantly been utilized for gas adsorption and separation. The abundant pore structure and high SSA provided active sites and adsorption spaces for gases. The presence of functional groups and various monomers endowed HCPs with superior adsorption capabilities for CO_2, H_2, CH_4, *etc.*

HCPs with an SSA of up to 803 m^2 g^{-1} were synthesized using waste foam plastic as precursor and FDA as cross-linking agent for CO_2 adsorption.[139] Under the conditions of 298 K and 10 bar, the adsorbents demonstrated a maximum adsorption capacity of 11.053 mmol g^{-1}. Using hydroxyl- and methoxy-substituted benzene as raw materials, a variety of O-rich HCPs were prepared which showed a CO_2 adsorption capacity of 64.1 mg g^{-1} at 0 °C.[60] Zhang *et al.* synthesized HCPs *via* a one-step Friedel–Crafts alkylation reaction, employing bipyridine and halobenzene as raw materials. By manipulating the structure and ratio of the monomers, the chemical composition and pore structure of the HCPs were adjusted. Due to the electrostatic interaction between bipyridine and the charge center of CO_2 molecules, the HCPs demonstrated

strong affinity to CO_2, with an adsorption capacity of 2.75 mmol g^{-1} at 273 K and 1 bar.[140]

HCPs relied on the physical adsorption of van der Waals forces to capture hydrogen molecules. The hydrogen storage capacity of the materials obeyed Chahine's law, indicating that an increase in SSA leads to improved hydrogen storage capacity. Consequently, it was imperative to optimize the SSA of HCPs. Fierro *et al.* synthesized high-SSA HCPs for H_2 storage using a "weaving" strategy, which demonstrated an absorption capacity of 2.1 wt% at 4 MPa and 77 K.[93] Although a high SSA enhanced the H_2 storage capacity, irreversible alterations in the porous structure occurred when the hydrogen storage pressure increased to 14 MPa. This resulted in a progressive decline in H_2 storage capacity with cycling, which might limit its application in high-pressure hydrogen storage. This meant that the material necessitated further structural optimization.

The incorporation of heteroatoms or functional groups into HCPs could modulate the interactions between adsorbates and the polymer matrix. This enhancement increased the gas adsorption efficiency of HCPs, thereby broadening their practical applications.[127]

4.2 Purification

HCPs had emerged as an exceptional porous material for water treatment and adsorption-based purification, attributed to the distinctive properties such as a high SSA, adjustability, biodegradability, and chemical versatility.

Peng *et al.* constructed a novel pyridine-modified hyper-crosslinked polystyrene adsorbent for blood purification through Friedel–Crafts alkylation and the subsequent cross-linking reactions.[28] The preparation method circumvented the issues associated with the toxic and carcinogenic chloromethyl ether used in traditional HCP resin synthesis. The results indicated that HCP (St-DVB-VP) possessed a highly porous network with an SSA of 761 m^2 g^{-1}. Significantly, the adsorbent demonstrated a superior adsorption performance for protein-bound toxins (bilirubin) and medium-to-large molecular weight toxins (PTH, IL-6) in *in vitro* experiments. Most importantly, the adsorbent demonstrated excellent blood compatibility.

The processability of HCPs at the macroscopic level has always been a challenge. The highly cross-linked in structure, insoluble and difficult to process properties of the polymers limited the practical applications of HCPs.[141–143] So, HCP gels are proposed as a promising means of molding and processing HCPs. As shown in Fig. 13, Gu *et al.* pioneered the synthesis of HCP gels by a thermally induced polymerization of tetrahedral monomers,[144] which possess hierarchical porosity as well as mechanical strength. The material was efficient in separating methylene blue and $KMnO_4$ from water contaminants, which further promotes the development of practical applications of HCPs.

4.3 Catalysis

HCPs can also be utilized for metal ion loading, acid–base functionalization, and other heterogeneous catalytic appli-
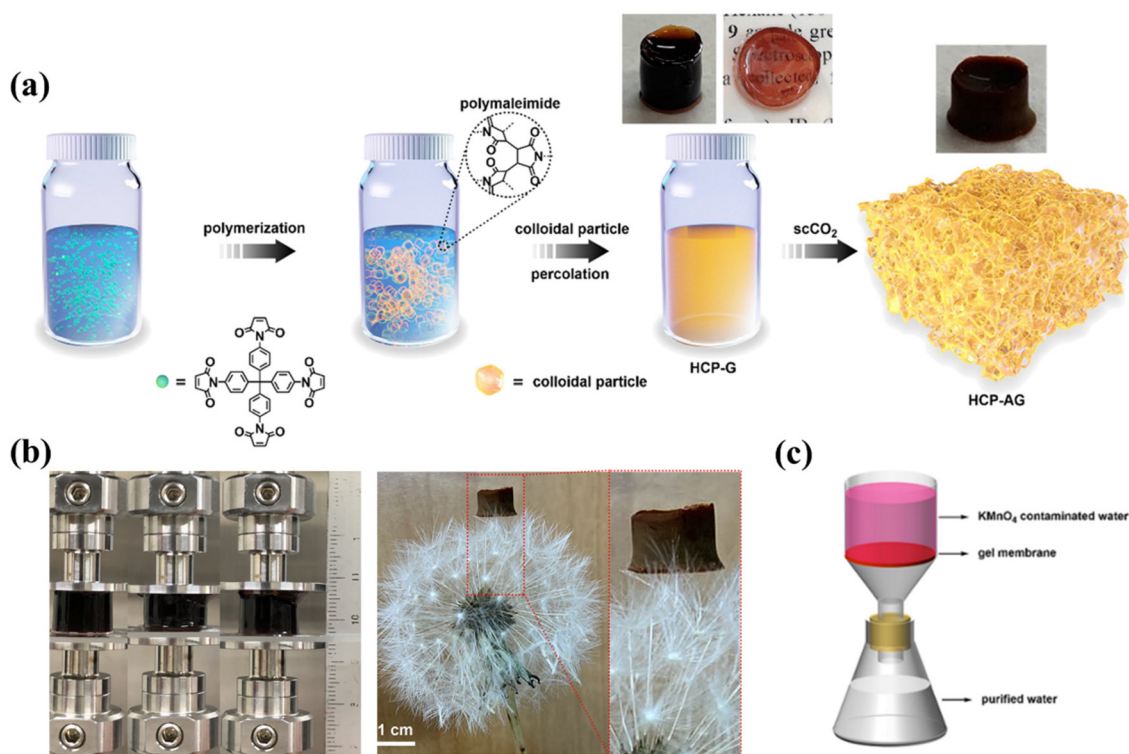

Fig. 13 (a) Synthesis of HCP gels and aerogels *via* gelation processes. (b) Photographs of HCP gels and aerogels. (c) The gel membrane separation system.[144] Copyright 2022, American Chemical Society.

cations due to their robust structure, superior physicochemical properties, high SSA, and ease of functionalization.

HCPs as catalyst support. Mondal et al. employed triphenylamine as the monomer and DBX as the cross-linker to fabricate porous organic polymers (PPN), with an SSA of 1165 m^2 g^{-1}. The abundant nitrogen content served as an anchor for Pd nanoparticles to facilitate the preparation of the Pd@PPN catalyst which demonstrated significant activity in the conversion of both saturated and unsaturated fatty acids into long-chain biofuel additives.[108] Li et al. successfully incorporated three analogous salen ligands into the polymer network via a Friedel–Crafts reaction, thereby modulating the SSA of the polymer.[61] The SSA obtained by post-polymerization were 700 m^2 g^{-1} (poly-salen-a), 484 m^2 g^{-1} (poly-salen-b), and 798 m^2 g^{-1} (poly-salen-c), respectively. Subsequently, they prepared the catalyst by anchoring Pd(II) onto the polymer. Notably, poly-salen-a-Pd exhibited superior performance in the Suzuki–Miyaura coupling reaction with various substrates.

In addition, the substituents of the HCPs significantly influenced the catalytic performance. Liu et al. introduced phenyl, 4-methoxyphenyl, 2-naphthyl, and other substituents at the 3,3′ positions of 1,1-bi-2-naphthol-derived phosphoric acids (BNPPAs) to create HCPs with distinct functionalities.[88] This approach involved BNPPA-based homochiral HCPs, which exhibited excellent thermal stability, chemical stability and a large SSA of 1098 m^2 g^{-1}. Furthermore, the chiral catalytic center within the polymer skeleton was highly adjustable, which demonstrated superior catalytic activity and selectivity.

Furthermore, HCPs were also widely used in photocatalysis. Based on the extended conjugation of the phenothiazine (PTZ) units in HCPs, photoinduced atom transfer radical polymeriz-ation (ATRP) showed high conversion and well-controlled molecular weight.[145] Gao et al. demonstrated an improved separation and transfer efficiency of photogenerated carriers by using HCPs prepared with monomers of different conjugated degrees.[74] HCPs with p-quaterphenyl (QP) as monomer showed excellent O_2 adsorption capacity and optimal photocatalytic activity of amines oxidation coupled with H_2O_2 generation. In addition, the type of crosslinker (DCM, DCE and DMB) determined the bandgap structure of HCPs photocatalysts, which played a critical role in the photocatalytic activity for amine oxidation and H_2O_2 production.[113]

4.4 Energy storage

In recent years, hypercrosslinked polymerization had attracted significant attention energy storage due to the simple synthesis process. HCPs can be used to prepare polymer-derived porous carbon with different structures and a high carbon residue. The derived porous carbons lead to a high SSA. The porous structures can be further modulated by designing precursor structures. Consequently, HCP-derived carbon materials, employing various strategies, displayed considerable potential in the field of electrochemical energy storage (Fig. 14a).[146]

Utilization of readily available monomers and cheap catalysts, such as $FeCl_3$, for the preparation of HCPs presented a cost-effective alternative to the noble metal catalysts. The HCPs could be directly employed as organic electrode materials (Fig. 14b). Through this economical synthetic route, a novel organic redox-active hypercrosslinked phenothiazine polymer was developed as organic cathodes in lithium-ion batteries, which exhibited a commendable capacity (0.5 C, 106 mA h g^{-1}).[147]
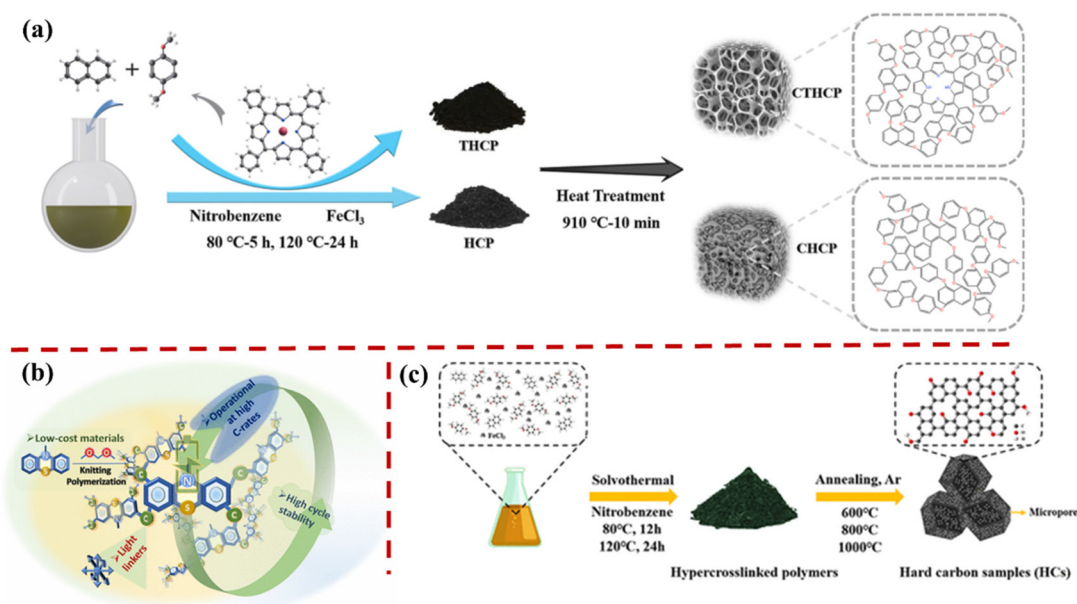

Fig. 14 (a) Synthesis of hyper-crosslinked polymer-based hard carbon samples.[146] Copyright 2024, Elsevier. (b) Hypercrosslinked phenothiazine polymer as an organic cathode for lithium batteries.[147] Copyright 2024, American Chemical Society. (c) Synthesis of hard carbon anodes for potassium-ion batteries.[119] Copyright 2022, American Chemical Society.

762 | RSC Appl. Polym., 2025, 3, 746–766

© 2025 The Author(s). Published by the Royal Society of Chemistry

HCPs can be used as a precursor of carbon for energy storage. One-dimensional tubular HCPs could be synthesized using triphenylamine as the monomer. Additionally, nitrogen-doped MnO/N-porous carbon nanotubes were produced through pyrolysis of polymer-loaded $Mn(CH_3COO)_2 \cdot 4H_2O$, demonstrating a reversible specific capacity of 652 mA h g^{-1} at 100 mA h g^{-1}.[62] These findings suggested that the composite of polymer-derived porous carbon was an optimal choice for high-performance energy storage devices. Furthermore, crosslinked polymerization, facilitated by Friedel–Crafts reactions using poly(styrene-divinylbenzene) (poly(St-DVB)) hollow particles as monomers, could preserve the hollow structure during pyrolysis. This process endowed the HCPs with abundant micropores and macropores, making them suitable for supercapacitors and lithium-ion batteries.[148] HCPs and the derived carbons with π-conjugated structures were constructed using benzene as monomer. Thanks to their highly cross-linked skeleton and conjugated structure, the carbon materials had a high SSA which was conductive as anode materials in lithium-ion with high reversible capacity.[116] On the other hand, the oxygen-containing functional groups in the HCPs prepared through DMB cross-linking using naphthalene as monomer could be regulated by changing the pyrolysis temperature, and they exhibited good electrochemical performance for potassium-ion storage (Fig. 14c).[119] Similarly, the porosity of HCPs constructed from simple monomers, such as biphenyl, could be tuned by varying the ratio of the monomer and FDA.[45] After pyrolysis, the obtained carbon material showed the specific capacity of up to 421 F g^{-1} at 1 A g^{-1} when served as an electrode material for supercapacitors. Using formaldehyde dimethyl acetal and 2,4,6-trichloro-1,3,5-triazine as cross-linking agents, HCPs prepared with 9,10-bis(diphenylmethylene)-9,10-dihydroanthracene (An-4Ph) as monomer exhibited good thermal stability and a high SSA (1000 m^2 g^{-1}). The materials could be directly used in supercapacitors, with high specific capacitance of 98.4 F g^{-1} at 0.5 A g^{-1} and good cyclic stability (95.3% after 200 cycles).[69]

Consequently, the structural design of enabled the preparation of HCPs suitable for direct energy storage. The pyrolysis altered the pore structure and functional groups of the as-synthesized materials, thereby expanding the scope of HCPs and the derived carbon materials in energy storage.

5 Summary and outlook

Hypercrosslinked polymers (HCPs) have been greatly developed in recent years due to the high specific surface area, good thermal stability and wide range of monomer sources. A variety of HCPs have been developed with structural regulation and functionalization design, which has led to a wide range of applications in various aspects such as gas adsorption, wastewater treatment, catalysis and energy storage.

Despite the advancements in the field of HCPs, several limitations remained. The synthesis of HCPs *via* external cross-linking required a diverse array of aromatic monomers to create polymers with adjustable pore structures. Although some characterization techniques (*e.g.*, solid-state NMR and gas adsorption and desorption tests) have been used, the structure of HCPs has not been fully explored. Precise control of the SSA and the pore structure by selecting appropriate monomers, solvents and cross-linkers remained an ongoing challenge. Furthermore, for the reaction systems, a detailed analysis of the factors affecting the SSA was essential. The evolution of pore size distribution remained unclear. Most current studies are application-driven and lack of depth in their research methodologies. So, there is a pressing to analyze the inherent structure of HCPs and the mechanisms underlying the porous formation and structural differences.

In addition, for the practical application of HCPs, the insolubility of most HCPs led to difficulties in processing. On the other hand, the side reactions of the Friedel–Crafts reaction as well as the large amount of released heat and corrosive gas were not conductive to the industrial production of HCPs. All these challenges will motivate researchers to promote the development and application of HCPs.

Author contributions

Conceptualization, Z. Y. L., Y. S., and S. J. W.; methodology, Z. Y. L., Y. S., and T. Y.; investigation, Z. Y. L., Z. H. M., and X. J. G.; writing – original draft, Z. Y. L. and Y. S.; writing – review & editing, Z. Y. L., Y. S., N. Z., S. J. W. and T. Y.; funding acquisition, Y. S., Z. J. L., T. Y. and X. D. T.

Data availability

Data availability is not applicable to this article as no new data were created or analyzed in this study.

Conflicts of interest

The authors declare no competing financial interest.

Acknowledgements

References

1 Y. Su, K.-i. Otake, J.-J. Zheng, H. Xu, Q. Wang, H. Liu, F. Huang, P. Wang, S. Kitagawa and C. Gu, *Nat. Commun.*, 2024, **15**, 144.

2 P. T. Phan, Q. T. Ta and P. K. Nguyen, *Polymers*, 2023, **15**, 887.

© 2025 The Author(s). Published by the Royal Society of Chemistry

RSC Appl. Polym., 2025, **3**, 746–766 | 763

3   Q. N. Tran, H. J. Lee and N. Tran, *Polymers*, 2023, **15**, 1279.

4   Y. Su, B. Li, H. Xu, C. Lu, S. Wang, B. Chen, Z. Wang, W. Wang, K.-i. Otake, S. Kitagawa, L. Huang and C. Gu, *J. Am. Chem. Soc.*, 2022, **144**, 18218–18222.

5   H. Zhang, W. Wei and K. A. I. Zhang, *Chem. Commun.*, 2023, **59**, 9167–9181.

6   L. Wang and H. Xu, *Prog. Polym. Sci.*, 2023, **145**, 101734.

7   C. Pathak, A. Gogoi, A. Devi and S. Seth, *Chem. – Eur. J.*, 2023, **29**, 202301512.

8   F. Topuz, M. H. Abdellah, P. M. Budd and M. A. Abdulhamid, *Polym. Rev.*, 2023, **64**, 251–305.

9   Q. Hao, Y. Tao, X. Ding, Y. Yang, J. Feng, R.-L. Wang, X.-M. Chen, G.-L. Chen, X. Li, H. OuYang, X. Hu, J. Tian, B.-H. Han, G. Zhu, W. Wang, F. Zhang, B. Tan, Z.-T. Li, D. Wang and L.-J. Wan, *Sci. China: Chem.*, 2023, **66**, 620–682.

10 S. Raza, S. Nazeer, A. Abid and A. Kanwal, *J. Polym. Res.*, 2023, **30**, 415.

11 R. Dawson, A. I. Cooper and D. J. Adams, *Prog. Polym. Sci.*, 2012, **37**, 530–563.

12 S. Xu, Y. Luo and B. Tan, *Macromol. Rapid Commun.*, 2013, **34**, 471–484.

13 J. Huang and S. R. Turner, *Polym. Rev.*, 2017, **58**, 1–41.

14 L. Tan and B. Tan, *Chem. Soc. Rev.*, 2017, **46**, 3322–3356.

15 J. Germain, J. M. J. Fréchet and F. Svec, *J. Mater. Chem.*, 2007, **17**, 4989–4997.

16 Y. Gu, S. U. Son, T. Li and B. Tan, *Adv. Funct. Mater.*, 2020, **31**, 2008265.

17 K. Cousins and R. Zhang, *Polymers*, 2019, **11**, 690.

18 V. A. Davankov and M. P. Tsyurupa, *Angew. Makromol. Chem.*, 1980, **91**, 127–142.

19 J. Germain, J. M. Frechet and F. Svec, *Small*, 2009, **5**, 1098–1111.

20 J. Hradil and E. Králová, *Polymer*, 1998, **39**, 6041–6048.

21 V. A. Davankov, M. M. Ilyin, M. P. Tsyurupa, G. I. Timofeeva and L. V. Dubrovina, *Macromolecules*, 1996, **29**, 8398–8403.

22 J.-H. Ahn, J.-E. Jang, C.-G. Oh, S.-K. Ihm, J. Cortez and D. C. Sherrington, *Macromolecules*, 2006, 627–632.

23 J. Y. Lee, C. D. Wood, D. Bradshaw, M. J. Rosseinsky and A. I. Cooper, *Chem. Commun.*, 2006, 2670–2672, DOI: **10.1039/b604625h**.

24 D. Zhang, L. Tao, J. Ju, Y. Wang, Q. Wang and T. Wang, *Polymer*, 2015, **60**, 234–240.

25 S. Wang, C. Zhang, Q. Liu and B. Tan, *Macromol. Rapid Commun.*, 2022, **43**, 2100449.

26 Y. Liu, S. Wang, X. Meng, Y. Ye, X. Song and Z. Liang, *Mater. Chem. Front.*, 2021, **5**, 5319–5327.

27 S. Wan, Q. Zou, J. Zhu, H. Luo, Y. Li, R. Abu-Reziq, J. Tang, R. Tang, C. Pan, C. Zhang and G. Yu, *Macromol. Rapid Commun.*, 2023, **44**, 202300340.

28 Y. Liu and X. Peng, *Front. Chem.*, 2022, **9**, 789814.

29 D. Jia, L. Ma, Y. Wang, W. Zhang, J. Li, Y. Zhou and J. Wang, *Chem. Eng. J.*, 2020, **390**, 124652.

30 Y. Gan, G. Chen, Y. Sang, F. Zhou, R. Man and J. Huang, *Chem. Eng. J.*, 2019, **368**, 29–36.

31 Z. Liu, Q. Mu, Y. Sun, P. Gao, Y. Yu, J. Gao, W. Shi, X. Wen and Z. Fei, *Colloids Surf., A*, 2020, **601**, 124996.

32 C. Xu, L. Jiang, X. Qin, C. Jin, L. Liu, S. Yu and M. Xian, *J. Taiwan Inst. Chem. Eng.*, 2019, **102**, 340–348.

33 C. Xu, W. Sun, X. Qin, C. Wang, S. Yu, M. Xian and H. Liu, *J. Chem. Technol. Biotechnol.*, 2019, **94**, 276–287.

34 Y. Wang, Y. Gan and J. Huang, *Ind. Eng. Chem. Res.*, 2020, **59**, 11275–11283.

35 Y. Meng, Y. Wang, L. Liu, Y. Fang, F. Ma, C. Zhang and H. Dong, *Colloids Surf., A*, 2022, **632**, 127644.

36 M. P. Tsyurupa and V. A. Davankov, *React. Funct. Polym.*, 2002, **53**, 193–203.

37 L. L. Bai, Y. H. Zhou, X. L. Wang, S. G. Yuan and X. L. Wu, *Chin. Chem. Lett.*, 2011, **22**, 1115–1118.

38 A. M. James, S. Harding, T. Robshaw, N. Bramall, M. D. Ogden and R. Dawson, *ACS Appl. Mater. Interfaces*, 2019, **11**, 22464–22473.

39 C. D. Wood, B. Tan, A. Trewin, H. Niu, D. Bradshaw, M. J. Rosseinsky, Y. Z. Khimyak, N. L. Campbell, R. Kirk, E. Stöckel and A. I. Cooper, *Chem. Mater.*, 2007, **19**, 2034–2048.

40 D. Fang, X. Li, M. Zou, X. Guo and A. Zhang, *Beilstein J. Org. Chem.*, 2019, **15**, 2856–2863.

41 R. T. Woodward, L. A. Stevens, R. Dawson, M. Vijayaraghavan, T. Hasell, I. P. Silverwood, A. V. Ewing, T. Ratvijitvech, J. D. Exley, S. Y. Chong, F. Blanc, D. J. Adams, S. G. Kazarian, C. E. Snape, T. C. Drage and A. I. Cooper, *J. Am. Chem. Soc.*, 2014, **136**, 9028–9035.

42 R. Dawson, T. Ratvijitvech, M. Corker, A. Laybourn, Y. Z. Khimyak, A. I. Cooper and D. J. Adams, *Polym. Chem.*, 2012, **3**, 2034–2038.

43 B. Li, R. Gong, Y. Luo and B. Tan, *Soft Matter*, 2011, **7**, 10910–10916.

44 M. P. Tsyurupa, Z. K. Blinnikova, Y. A. Davidovich, S. E. Lyubimov, A. V. Naumkin and V. A. Davankov, *React. Funct. Polym.*, 2012, **72**, 973–982.

45 A. Varyambath, W. L. Song, S. Singh, J. S. Kim and I. Kim, *Microporous Mesoporous Mater.*, 2021, **312**, 110800.

46 C. Liu, X. Ma, P. Du and Z. Rao, *Chem. Eng. Sci.*, 2020, **216**, 115477.

47 A. Giri, S. Biswas, M. W. Hussain, T. K. Dutta and A. Patra, *ACS Appl. Mater. Interfaces*, 2022, **14**, 7369–7381.

48 L. Zhang, T. Sun, Y. Dong, Z. Fang and Y. Xu, *Sci. Bull.*, 2022, **67**, 1416–1420.

49 H. Masoumi, A. Ghaemi and H. G. Gilani, *Sep. Purif. Technol.*, 2021, **260**, 118221.

50 Y. Ahmadi and K.-H. Kim, *Polym. Rev.*, 2022, **63**, 365–393.

51 A. Waheed, N. Baig, N. Ullah and W. Falath, *J. Environ. Manage.*, 2021, **287**, 112360.

52 C. Zhang, R. Kong, X. Wang, Y. Xu, F. Wang, W. Ren, Y. Wang, F. Su and J.-X. Jiang, *Carbon*, 2017, **114**, 608–618.

53 R. Thanchanok, *J. Polym. Environ.*, 2020, **28**, 2211–2218.

54 Z. Liu, J. Wang, Y. Guo, J. Liu, J. Wang, C. Wang, Q. Wu and Z. Wang, *J. Chromatogr., A*, 2022, **1676**, 463206.

55 P. Su, X. Zhang, Z. Xu, G. Zhang, C. Shen and Q. Meng, *New J. Chem.*, 2019, **43**, 17267–17274.

© 2025 The Author(s). Published by the Royal Society of Chemistry

56 Z. Xu, M. Rong, Q. Meng, H. Yao, S. Ni, L. Wang, H. Xing, H. Qu, L. Yang and H. Liu, *Chem. Eng. J.*, 2020, **400**, 125991.

57 C. Yan, Y. Wu, H. Lu, H. Liu, G. Yi, M. Li, X. Cai, S. Gao and Z. Yang, *Microporous Mesoporous Mater.*, 2022, **343**, 112157.

58 L. Zhou, K. Chai, X. Yao and H. Ji, *Chem. Eng. J.*, 2021, **418**, 129351.

59 M. Ansari, A. Hassan, A. Alam and N. Das, *Microporous Mesoporous Mater.*, 2021, **323**, 111242.

60 L. Shao, N. Liu, L. Wang, Y. Sang, H. a. Wan, P. Zhan, L. Zhang, J. Huang and J. Chen, *Chemosphere*, 2022, **288**, 132499.

61 J. Bi, Y. Dong, D. Meng, D. Zhu and T. Li, *Polymer*, 2019, **164**, 183–190.

62 P. Mu, W. Ma, Y. Zhao, C. Zhang, S. Ren, F. Wang, C. Yan, Y. Chen, J. H. Zeng and J.-X. Jiang, *J. Power Sources*, 2019, **426**, 33–39.

63 E. M. Maya, A. Valverde-Gonzalez and M. Iglesias, *Molecules*, 2020, **25**, 4598.

64 Y. Cheng, S. Razzaque, Z. Zhan and B. Tan, *Chem. Eng. J.*, 2021, **426**, 130731.

65 Q. Peng, H. Zhao, G. Chen, Q. Yang, X. Cao, S. Xiong, A. Xiao, G. Li, B. Liu and Q. Liu, *J. Environ. Manage.*, 2023, **339**, 117763.

66 S. Ravi, Y. Choi, S. Wu, R. Xiao and Y.-S. Bae, *Environ. Sci.: Nano*, 2022, **9**, 730–741.

67 C. Liu, W. Xu, D. Xiang, Q. Luo, S. Zeng, L. Zheng, Y. Tan, Y. Ouyang and H. Lin, *Catal. Lett.*, 2020, **150**, 2558–2565.

68 M. R. Moradi, H. R. Penchah and A. Ghaemi, *Can. J. Chem. Eng.*, 2023, **101**, 24887.

69 M. G. Mohamed, X. Zhang, T. H. Mansoure, A. F. M. El-Mahdy, C.-F. Huang, M. Danko, Z. Xin and S.-W. Kuo, *Polymer*, 2020, **205**, 122857.

70 Y. Tian, Y. Wang, L. Liu, H. Dong, X. Zhu, F. Ma and C. Zhang, *J. Mol. Liq.*, 2023, **372**, 121171.

71 X. Zeng and J. Huang, *J. Colloid Interface Sci.*, 2020, **569**, 177–183.

72 Y. Tian, L. Liu, F. Ma, X. Zhu, H. Dong, C. Zhang and F. Zhao, *J. Hazard. Mater.*, 2021, **419**, 126538.

73 C. Liu, Y. Li, M. Zhang, K. Yuan, S. Liang, G. Yu, Z. Weng and X. Jian, *Eur. Polym. J.*, 2020, **130**, 109674.

74 X. Nie, Y. Zhao, W. Gao, W. Liu, X. Cheng, Y. Gao, N. Shang, S. Gao and C. Wang, *Chem. – Eur. J.*, 2023, **29**, 202203607.

75 A. Modak, S. Das, D. K. Chanda, A. Samanta and S. Jana, *New J. Chem.*, 2019, **43**, 3341–3349.

76 Z. Zhu, J. Cui, X. Cao, L. Yang, H. Sun, W. Liang, J. Li and A. Li, *Int. J. Hydrogen Energy*, 2022, **47**, 9504–9516.

77 F. Liu, W. Liang, C. Wang, J. He, C. Xiao, Z. Zhu, H. Sun and A. Li, *Sol. Energy Mater. Sol. Cells*, 2021, **221**, 110913.

78 A. E. Sadak, *Microporous Mesoporous Mater.*, 2021, **311**, 110727.

79 H. R. Penchah, A. Ghaemi and H. G. Gilani, *Energy Fuels*, 2019, **33**, 12578–12586.

80 H. Masoumi, A. Ghaemi and H. G. Gilani, *J. Hazard. Mater.*, 2021, **416**, 125923.

81 W. Liu, J. Wang, J. Liu, F. Hou, Q. Wu, C. Wang and Z. Wang, *J. Chromatogr., A*, 2020, **1628**, 461470.

82 J. Bai, S. Li, X. Ma, H. Yan, S. Su, S. Wang and J. Wang, *Microporous Mesoporous Mater.*, 2022, **331**, 111647.

83 Y. Liu, X. Jia, J. Liu, X. Fan, B. Zhang, A. Zhang and Q. Zhang, *Appl. Organomet. Chem.*, 2019, **33**, 5025.

84 A. E. Sadak, E. Karakus, Y. M. Chumakov, N. A. Dogan and C. T. Yavuz, *ACS Appl. Energy Mater.*, 2020, **3**, 4983–4994.

85 Q. Ou, Q.-M. Zhang, P.-C. Zhu, Q.-P. Zhang, Z. Cheng and C. Zhang, *Eur. Polym. J.*, 2019, **120**, 109216.

86 R. Liu, Z. Yang, S. Chen, J. Yao, Q. Mu, D. Peng and H. Zhao, *Eur. Polym. J.*, 2019, **119**, 94–101.

87 L. Yao, L. Zhang, B. Long, Y. Dai and Y. Ding, *J. Mol. Liq.*, 2021, **325**, 115002.

88 Y. Zhang, Z. Zhang, S. Ma, J. Jia, H. Xia and X. Liu, *J. Mater. Chem. A*, 2021, **9**, 25369–25373.

89 Z. Yang, S. Fu, C. Yan, J. Yao and W. Liu, *J. Macromol. Sci., Part A*, 2019, **56**, 162–169.

90 J. Bai, W. Zhang, X. Ma, L. Chen, L. Liu and C. Zhang, *Microporous Mesoporous Mater.*, 2020, **294**, 109892.

91 W.-K. An, S.-J. Zheng, H.-X. Zhang, T.-T. Shang, H.-R. Wang, X.-J. Xu, Q. Jin, Y. Qin, Y. Ren, S. Jiang, C.-L. Xu, M.-S. Hou and Z. Pan, *Green Chem.*, 2021, **23**, 1292–1299.

92 L. Zhang, L. Yao, L. Ye, B. Long, Y. Dai and Y. Ding, *J. Environ. Chem. Eng.*, 2020, **8**, 104562.

93 P. Ramirez-Vidal, F. Suarez-Garcia, R. L. S. Canevesi, A. Castro-Muniz, P. Gadonneix, J. I. Paredes, A. Celzard and V. Fierro, *J. Colloid Interface Sci.*, 2022, **605**, 513–527.

94 X. Dong, A. Akram, B. Comesana-Gandara, X. Dong, Q. Ge, K. Wang, S.-P. Sun, B. Jin and C. H. Lau, *ACS Appl. Polym. Mater.*, 2020, **2**, 2586–2593.

95 P. Najafi, H. R. Penchah and A. Ghaemi, *Environ. Technol. Innovation*, 2021, **23**, 101746.

96 M. Sun, C. Yan, Y. Wu, M. Li, S. Chen and Z. Yang, *J. Mater. Sci.*, 2022, **57**, 13800–13813.

97 Y. An, X. Meng, S. Li, Q. Wang, W. Liu, L. Hao, X. Yang, C. Wang, Z. Wang and Q. Wu, *Food Chem.*, 2022, **389**, 133121.

98 Z. Wang, Y. Huang, Y. Hu, S. Peng, X. Peng, Z.-W. Li, J. Zheng, F. Zhu and G. Ouyang, *Microchem. J.*, 2022, **179**, 107535.

99 F. Liu, W. Liang, J. He, Y. Lei, Z. Tian, H. Sun, J. Li, Z. Zhu and A. Li, *Polymer*, 2021, **231**, 124115.

100 X. Wang, P. Mu, C. Zhang, Y. Chen, J. Zeng, F. Wang and J.-X. Jiang, *ACS Appl. Mater. Interfaces*, 2017, **9**, 20779–20786.

101 Z. Yao, W. Jinrong and Z. Jing, *China Plast. Ind.*, 2022, **50**, 27–32.

102 R. M. N. Kalla, S. S. Reddy and I. Kim, *Catal. Lett.*, 2019, **149**, 2696–2705.

103 M. Bauza, G. T. Palomino and C. P. Cabello, *Sep. Purif. Technol.*, 2022, **303**, 122211.

© 2025 The Author(s). Published by the Royal Society of Chemistry

RSC Appl. Polym., 2025, **3**, 746–766 | **765**

104 J.-S. M. Lee, T. Kurihara and S. Horike, *Chem. Mater.*, 2020, **32**, 7694–7702.

105 C. Wang, Y. An, Z. Li, Q. Wang, W. Liu, L. Hao, Z. Wang and Q. Wu, *Food Chem.*, 2022, **396**, 133694.

106 S. Ghosh, A. Ghosh, S. Riyajuddin, S. Sarkar, A. H. Chowdhury, K. Ghosh and S. M. Islam, *ChemCatChem*, 2020, **12**, 1055–1067.

107 D. Wang, G. Chen, X. Li and Q. Jia, *Sep. Purif. Technol.*, 2019, **227**, 115720.

108 C. Sarkar, S. C. Shit, D. Q. Dao, J. Lee, N. H. Tran, R. Singuru, K. An, D. N. Nguyen, Q. V. Le, P. N. Amaniampong, A. Drif, F. Jerome, P. T. Huyen, T. T. N. Phan, D.-V. N. Vo, N. T. Binh, Q. T. Trinh, M. P. Sherburne and J. Mondal, *Green Chem.*, 2020, **22**, 2049–2068.

109 Y. Wang, Z. Shu, X. Zeng, W. Kuang and J. Huang, *Ind. Eng. Chem. Res.*, 2020, **59**, 11705–11712.

110 Y. Sang and J. Huang, *Chem. Eng. J.*, 2020, **385**, 123973.

111 W. Zhang, F. Ma, L. Ma, Y. Zhou and J. Wang, *ChemSusChem*, 2020, **13**, 341–350.

112 M. G. Mohamed, A. F. M. El-Mahdy, T.-S. Meng, M. M. Samy and S.-W. Kuo, *Polymers*, 2020, **12**, 2426.

113 W. Wang, W. Gao, X. Nie, W. Liu, X. Cheng, N. Shang, S. Gao and C. Wang, *J. Colloid Interface Sci.*, 2022, **616**, 1–11.

114 Q. Wang, C. Wang, J. Wang, W. Liu, L. Hao, J. Zhou, Z. Wang and Q. Wu, *Food Chem.*, 2020, **317**, 126410.

115 H.-Y. Kong, T.-X. Wang, Y. Tao, X. Ding and B.-H. Han, *Sep. Purif. Technol.*, 2022, **290**, 120805.

116 Z. Guo, X. Tian, Y. Song, T. Yang, Z. Ma, X. Gong and C. Wang, *Coatings*, 2023, **13**, 421.

117 R.-Y. Yan, W.-H. Lin, T.-L. Lu and J.-L. Chen, *Spectrochim. Acta, Part A*, 2023, **291**, 122383.

118 E. Cucu, E. Dalkilic, R. Altundas and A. E. Sadak, *Microporous Mesoporous Mater.*, 2022, **330**, 111567.

119 Z. Liu, S. Wu, Y. Song, T. Yang, Z. Ma, X. Tian and Z. Liu, *ACS Appl. Mater. Interfaces*, 2022, **14**, 47674–47684.

120 S. Razzaque, L. Guo, J. Weng, L. Su and B. Tan, *J. Colloid Interface Sci.*, 2022, **620**, 94–106.

121 Y. Luo, Z. Yang, X. Suo, H. Chen, T. Wang, Z. Wang, Y. Liu, Y. Lyu, I. Popovs and S. Dai, *Nano Res.*, 2021, **14**, 3282–3287.

122 K. Soukupová and K. Jeřábek, *Polym. Bull.*, 2022, **79**, 10757–10764.

123 C. D. Wood, B. Tan, A. Trewin, F. Su, M. J. Rosseinsky, D. Bradshaw, Y. Sun, L. Zhou and A. I. Cooper, *Adv. Mater.*, 2008, **20**, 1916–1921.

124 G. Paul, F. Begni, A. Melicchio, G. Golemme, C. Bisio, D. Marchi, M. Cossi, L. Marchese and G. Gatti, *ACS Appl. Polym. Mater.*, 2019, **2**, 647–658.

125 L. Zhang, H. Yang and H. Zhang, *Microporous Mesoporous Mater.*, 2022, **342**, 112118.

126 G. Feng, M. Yang, H. Chen, B. Liu, Y. Liu and H. Li, *Sep. Purif. Technol.*, 2023, **323**, 124484.

127 S. Hou, J. Hu, X. Liang, D. Zhang and B. Tan, *J. Mater. Chem. A*, 2022, **10**, 15062–15073.

128 B. Liu, C. Mao, Z. Zhou, Q. Wang, X. Zhou, Z. Liao, R. Deng, D. Liu, J. Beiyuan, D. Lv, J. Li, L. Huang, X. Chen and W. Yuan, *Int. J. Mol. Sci.*, 2023, **24**, 370.

129 J. Wen, L. Xiao, T. Sun, Z. Lei, H. Chen and H. Li, *Microporous Mesoporous Mater.*, 2021, **319**, 111069.

130 Y. Luo, S. Zhang, Y. Ma, W. Wang and B. Tan, *Polym. Chem.*, 2013, **4**, 1126–1131.

131 T.-X. Wang, X. Ding and B.-H. Han, *Polymer*, 2022, **259**, 125344.

132 L. Liu, Y. Fang, Y. Meng, X. Wang, F. Ma, Z. Zhang and H. Dong, *Desalination*, 2020, **478**, 114300.

133 M. S. Ramezani, J. Ozdemir, A. R. Khosropour and M. H. Beyzavi, *ACS Appl. Mater. Interfaces*, 2020, **12**, 44117–44124.

134 T.-N. Gao, T. Wang, W. Wu, Y. Liu, Q. Huo, Z.-A. Qiao and S. Dai, *Adv. Mater.*, 2019, **31**, 1806254.

135 W. Song, Y. Zhang, A. Varyambath and I. Kim, *ACS Nano*, 2019, **13**, 11753–11769.

136 Q. Li, S. Jin and B. Tan, *Sci. Rep.*, 2016, **6**, 31359.

137 J. Wang, H. Yu, Z. Yang, A. Zhang, Q. Zhang and B. Zhang, *Carbon*, 2019, **152**, 255–266.

138 A. Varyambath, M.-R. Kim and I. Kim, *New J. Chem.*, 2018, **42**, 12745–12753.

139 F. Maleki, A. Ghaemi and G. M. M. Sadeghi, *Environ. Prog. Sustainable Energy*, 2023, **42**, 13954.

140 C. Li, H. Cai, X. Yang, F. Liu, C. Yang, P. Chen, Z. Chen and T. Zhao, *J. CO2 Util.*, 2022, **64**, 102203.

141 L. Wang, Y. Su and C. Gu, *Acc. Mater. Res.*, 2022, **3**, 1049–1060.

142 B. Chen, Y. Kuang, L. Liu, L. Cai, Z. Wang, P. Yin, L. Huang and C. Gu, *CCS Chem.*, 2024, **6**, 1767–1775.

143 Y. Su, B. Li, Z. Wang, A. Legrand, T. Aoyama, S. Fu, Y. Wu, K.-I. Otake, M. Bonn, H. I. Wang, Q. Liao, K. Urayama, S. Kitagawa, L. Huang, S. Furukawa and C. Gu, *J. Am. Chem. Soc.*, 2024, **146**, 15479–15487.

144 Y. Su, Z. Wang, A. Legrand, T. Aoyama, N. Ma, W. Wang, K.-i. Otake, K. Urayama, S. Horike, S. Kitagawa, S. Furukawa and C. Gu, *J. Am. Chem. Soc.*, 2022, **144**, 6861–6870.

145 S. Dadashi-Silab, F. Lorandi, M. J. DiTucci, M. Sun, G. Szczepaniak, T. Liu and K. Matyjaszewski, *J. Am. Chem. Soc.*, 2021, **143**, 9630–9638.

146 Z.-h. Ma, T. Yang, Y. Song, X.-d. Tian, Z.-y. Liu, X.-j. Gong and Z.-j. Liu, *J. Colloid Interface Sci.*, 2024, **661**, 436–449.

147 H. Bildirir, D. Alván, N. Patil, V. A. de la Peña O'Shea, M. Liras and R. Marcilla, *ACS Appl. Polym. Mater.*, 2024, **6**, 10092–10101.

148 Y. Kawai and T. Yamamoto, *Adv. Powder Technol.*, 2020, **31**, 614–620.

149 E. S. Bakhvalova, A. V. Bykov, M. E. Markova, Y. V. Lugovoy, A. I. Sidorov, V. P. Molchanov, M. G. Sulman, L. Kiwi-Minsker and L. Z. Nikoshvili, *Molecules*, 2023, **28**, 4938.